UC Irvine
UC Irvine Previously Published Works

Title
Neutron sawtooth behavior in the PLT, DIII-D, and TFTR tokamaks

Permalink
https://escholarship.org/uc/item/2c66n2wt

Journal
Physics of Plasmas, 1(4)

ISSN
1070-664X

Authors
Lovberg, JA
Heidbrink, WW
Strachan, JD
et al.

Publication Date
1989-04-01

DOI
10.1063/1.859012

Copyright Information
This work is made available under the terms of a Creative Commons Attribution License, availalbe at https://creativecommons.org/licenses/by/4.0/

Peer reviewed

eScholarship.org Powered by the California Digital Library
University of California

Neutron sawtooth behavior in the PLT, DIII-D, and TFTR tokamaks

J. A. Lovberg,[a] W. W. Heidbrink,[b] J. D. Strachan, and V. S. Zaveryaev[c]
Plasma Physics Laboratory, Princeton University, Princeton, New Jersey 08543

(Received 4 August 1988; accepted 5 December 1988)

The effect of the sawtooth instability on the 2.5 MeV neutron emission in the PLT [*Plasma Physics Controlled Nuclear Fusion Research, 1976* (IAEA, Vienna, 1977), Vol. I, p. 21], DIII-D [*Plasma Physics Controlled Nuclear Fusion Research, 1986* (IAEA, Vienna, 1987), Vol. 1, p. 159], and TFTR [*Plasma Physics Controlled Nuclear Fusion Research, 1984* (IAEA, Vienna, 1985), Vol. I, p. 29] tokamaks is studied. In thermonuclear plasmas, the instability typically results in a 20% reduction in emission. The time evolution of the thermonuclear neutron signal suggests that the sawtooth crash consists of four phases. First, the electron density profile flattens rapidly (in approximately 30 μsec on PLT) but, in some cases, there is little associated change in neutron emission, suggesting that most reacting ions remain confined in the sawtooth region but do not completely mix. After the electron sawtooth, the ions continue to mix, resulting in an approximate 10% reduction in neutron emission in about 0.5 msec. The emission then decays more slowly during the final two phases. Thermalization of reacting ions on an approximate $3\tau_{ii}$ time scale accounts for only about 20% of the slow drop. Most of the slow drop seems to be caused by loss of ion energy from the mixing region (an ion heat pulse).

I. INTRODUCTION

An understanding of the effect of the sawtooth instability on ions is important in studies of ion transport and in calculations of the performance of proposed ignition experiments.[1] Sawtooth behavior in the 2.45 MeV neutron emission was observed previously on the Alcator-A,[2] TFR,[3] and JET[4] tokamaks and, more recently, in collimated neutron measurements on JET.[5] Sawteeth in the central ion temperature have been measured with x-ray spectroscopy on TFTR[6] and with charge-exchange recombination spectroscopy on PBX.[7] On PBX, time-resolved measurements showed that the ion temperature profile flattens at the sawtooth.[7] Flattening of the density profiles of impurity ions at sawteeth was observed on Alcator C.[8]

In our work, the temporal resolution ($\gtrsim 10$ kHz) of the neutron measurements was faster than the observed decay rates, permitting a more-detailed study of the temporal behavior of ions at sawteeth than was possible in earlier studies. The paper has two main aims. One is to catalog the effect of sawteeth on the neutron source strength in tokamaks. Thermonuclear neutron data from the PLT,[9] DIII-D,[10] and TFTR[11] tokamaks have been obtained with similar instrumentation under a wide range of operating conditions in plasmas with Ohmic heating alone, hydrogen neutral beam injection into L-mode and H-mode plasmas, ion cyclotron resonance heating (ICRH), and pellet injection. In a wide variety of plasmas, similar behavior is observed. Generally, a rapid initial drop in emission is observed, followed by a slower decay. The initial drop in emission often takes longer than the electron temperature sawtooth. The time scale of the slower drop depends on machine size, varying approximately as the minor radius squared (a^2). The total drop in neutron emission $\Delta I_n/I_n$ is usually larger than the reduction in central electron temperature $\Delta T_e/T_e$.

The second major aim is to explain the neutron signal by considering possible ion behavior at the sawtooth. Four processes are identified. First, on the time scale of the electron sawtooth, the ion density must flatten with the electron density to preserve quasineutrality; however, the neutron emission drops gradually as though hot deuterons respond more slowly than electrons. Second, after the electron sawtooth, the ion velocity-space distribution is blended in an "ion mixing" phase and the emission falls approximately 10%. Generally, the density crash and mixing phases are too short for significant classical energy loss by the reacting ions. In the third phase, the hot ions that produce the reactions begin to thermalize, but the time scale is sufficiently long that, in some plasmas, a Maxwellian distribution may never be established. Concurrently, in the fourth process, the plasma responds to the flattened density and "temperature" profiles. At the edge of the mixing region, a steep gradient exists and rapid transport occurs. Both thermalization and diffusion result in a further $\sim 10\%$ reduction in emission on a 10 msec time scale. In our analysis, the "transport" and "thermalization" phases terminate when the neutron emission ceases to drop as the plasma reheats and the density peaks.

The paper is organized as follows. The temporal resolution of the detectors and the plasma conditions are discussed in Sec. II. Thermonuclear neutron data from PLT, DIII-D, and TFTR are presented in Sec. III. Next, the expected behavior during the electron crash phase (Sec. IV A), mixing phase (Sec. IV B), thermalization phase (Sec. IV C), and transport phase (Sec. IV D) is compared with the data. We conclude (Sec. V) that (i) hot ions are not mixed uniformly throughout the sawtooth region during the electron crash phase but may be mixed on a longer time scale, (ii) thermalization probably does not play a dominant role in the ob-

[a] Present address: Maxwell Laboratories, Inc., San Diego, California.
[b] Present address: Department of Physics, University of California, Irvine, California 92717.
[c] Present address: I. V. Kurchatov Institute of Atomic Energy, Moscow, USSR.

 0899-8221/89/040874-19$01.90 © 1989 American Institute of Physics

served temporal evolution, and (iii) an ion heat pulse escapes from the center of the plasma. Finally, in two appendices, it is shown that neutron and 15 MeV proton data from beam–plasma reactions are consistent with our interpretation of the thermonuclear data.

II. APPARATUS

A. Neutron diagnostics

Fast neutron detectors[12,13] that utilize uncollimated plastic scintillators mounted close to the tokamak were the primary diagnostics for this study. Similar detectors were used on all three machines. Neutrons strike a plastic scintillator producing recoil protons that cause the plastic to scintillate. The light travels by internal reflection down an acrylic rod to a shielded photomultiplier operated in current mode. The photomultiplier signal is digitized by a transient digitizer. Generally, three factors limit the temporal response of the detectors: counting statistics, amplifier/digitizer frequency response, and neutron scattering. The intrinsic response of the plastic scintillator is $<0.1\,\mu$sec. However, at low levels of neutron emission, the signal-to-noise ratio is degraded by statistical fluctuations in the number of neutrons that collide with the scintillator which results in poorer temporal resolution. Also, on TFTR, electrical noise placed a lower limit on the useful signal level. When an adequate signal existed, the frequency response of the detectors was limited by the photomultiplier amplifier to approximately 20 kHz on PLT and TFTR and to approximately 100 kHz on DIII-D. The digitizer sampling rate was 100 kHz on PLT and DIII-D and 20 kHz on TFTR.

The frequency response of the detectors was nominally 20 kHz, but there is an additional factor that could degrade the resolution further: neutron scattering. If detected in appreciable numbers, neutrons that bounce around the tokamak hall could significantly degrade the frequency response. To minimize this effect, the detectors were placed close to the machine between toroidal field coils. On TFTR, the scintillator was mounted directly behind a 1.3 cm thick stainless steel vacuum flange at the horizontal midplane. On DIII-D, the scintillator was mounted normal to a 2.5 cm thick stainless steel flange that is 85 cm above the horizontal midplane. Similar results to the ones reported here were obtained with the scintillator on the horizontal midplane. On PLT, the scintillator was mounted approximately 1 m away from the vacuum vessel near the midplane. Each of these installations has a different geometry for neutron scattering. Detailed scattering calculations have not been performed, but it is thought that scattering does not significantly degrade the frequency response since neutron transients as rapid as $\dot{I}_n/I_n = 0.8\ \text{msec}^{-1}$ (which is about four times faster than the transients reported here) have been observed during high-beta instabilities.[14,15] Also, when the plasma center moved 83 cm during compression on TFTR[16] and approximately 20 cm during the fishbone instability on PDX,[14] the magnitude of the neutron emission changed as expected for a virgin (unscattered) source. These observations suggest that neutron scattering does not limit the frequency response of our measurements.

On all three tokamaks, neutron measurements with the plastic scintillators were corroborated by slower measurements (approximately 0.2 msec resolution) made with adjacent ZnS(^{6}Li) scintillators.[13] The measurements also were consistent with measurements made with BF_3 proportional counters (PLT and DIII-D) and fission detectors (TFTR).

B. Tokamak conditions

The PLT sawtooth observations used in this study were made during a series of high-power ^{3}He-minority ICRH runs in late 1984 and early 1985. Discharges in the database have the parameter ranges $I_p = 500$–600 kA, $B_t = 31$–33 kG, $\bar{n}_e = 2$–$4\times10^{13}\ \text{cm}^{-3}$, and $T_{e0} = 2.0$–3.2 keV. In addition to neutron data, the database includes electron temperature and density profiles from Thomson scattering, Z_{eff} inferred from a central-chord visible bremsstrahlung measurement, and fractional changes in central electron temperature and line-averaged electron density at the sawtooth from electron cyclotron emission (ECE) and microwave interferometry. Additional observations on PLT were made in $H^0 \rightarrow D^+$ neutral-beam-heated plasmas, in H-minority ICRH-heated deuterium plasmas, and in Ohmically heated deuterium plasmas.

The TFTR observations were made during the spring 1985 run period and include sawteeth in full size ($a \simeq 81$ cm; $R_0 \simeq 255$ cm) plasmas with $I_p = 0.8$–2.2 MA, $B_t = 4.0$–4.8 T, $\bar{n}_e = 2$–$6\times10^{13}\ \text{cm}^{-3}$, and $T_e(0) = 1.8$–3.5 keV. Some of the plasmas were fueled with pellets and some with gas. About 70 sawteeth for which concurrent Thomson scattering data and soft x-ray (SXR) measurements of the sawtooth inversion radius were available were selected for inclusion in a database. Subordinate relaxations[17] were excluded from the study, although they were observed to correlate with small (approximately 2%) reductions in neutron emission. In addition to neutron data, the database included Z_{eff} inferred from a central visible bremsstrahlung chord, the fractional change in central SXR emission $\Delta A/A$ and central electron temperature $\Delta T_e/T_e$ (from ECE), the magnitude of and fractional change in line-averaged density $\Delta\bar{n}_e/\bar{n}_e$, the shape of the electron temperature and density profiles (from Thomson scattering), and the central ion temperature inferred from Doppler broadening of the Ti K_α line.

Data from DIII-D were obtained in 1987 during $H^0 \rightarrow D^+$ beam injection over the parameter range $I_p = 0.7$–1.8 MA, $B_t = 1.0$–2.1 T, $\bar{n}_e = 3$–$12\times10^{13}\ \text{cm}^{-3}$, and $P_b \lesssim 10$ MW. Most of the plasmas were divertor discharges and many were H-mode[18] plasmas. The reduction in central electron temperature at a sawtooth was measured using ECE and SXR measurements gave the time evolution of the electron sawtooth.

An assumption of our analysis is that the neutron emission is thermonuclear. For Ohmic, $H^0 \rightarrow D^+$ beam, and ^{3}He- or H-minority ICRH heating, the deuterium population is thought to be heated only through collisions with electrons, energetic protons, or energetic ^{3}He ions, so the deuterium distribution is expected to be nearly Maxwellian. Central ion temperatures inferred from charge-exchange spectra and Doppler broadening of impurity lines are generally consistent with the temperature inferred from the neutron flux

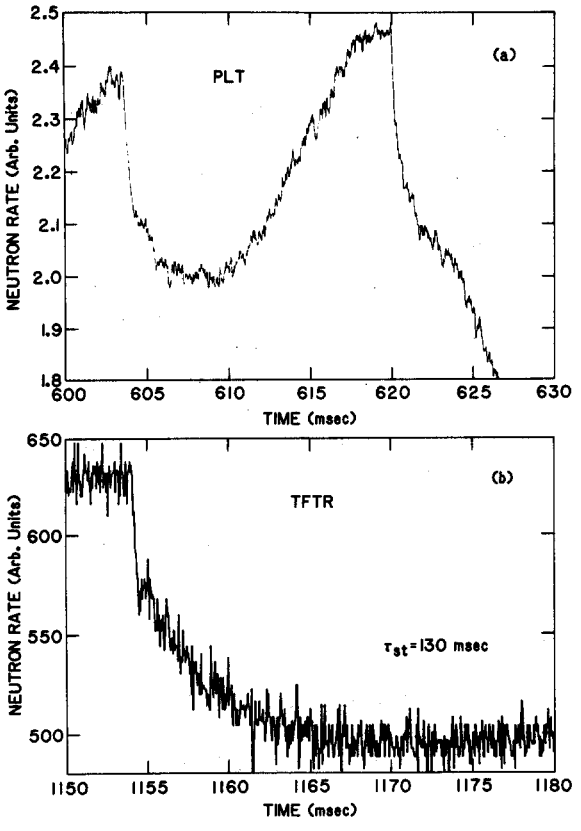

FIG. 1. Sawtooth in the neutron emission on (a) a PLT discharge with 3.2 MW ICRH heating in a ^{3}He-minority plasma with $B_t = 33.2$ kG, $I_p = 580$ kA, $T_{e0} = 2.7$ keV, $\bar{n}_e = 3.6\times10^{13}$ cm^{-3}, and $Z_{eff} = 3.0$ (ICRH shutoff at 630 msec); and (b) a TFTR Ohmic discharge with $B_t = 471.1$ kG, $I_p = 2.2$ MA, $T_{e0} = 2.9$ keV, $\bar{n}_e = 3.9\times10^{13}$ cm^{-3}, and $Z_{eff} = 2.2$. The initial drop rates and magnitudes are comparable, while the peak-to-trough time is approximately four times longer on TFTR, and the TFTR sawtooth period (approximately 130 msec) is about eight times longer.

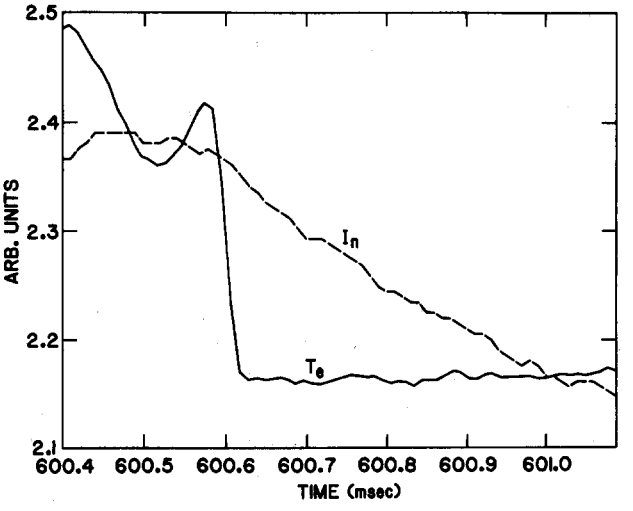

FIG. 2. Neutron sawtooth and concurrent electron temperature sawtooth for a 3.2 MW ICRH discharge on PLT with $B_t = 33.2$ kG, $I_p = 580$ kA, $\bar{n}_e = 3.6\times10^{13}$/cm^3, and a 3% ^{3}He minority. The average central electron temperature is $T_{e0} = 2.6$ keV, while the average central ion temperature inferred from the neutron emission is $T_{d0} = 3.2$ keV. The electron temperature drop time is about 30 μsec, compared with an initial drop time of about 550 μsec for the neutrons.

assuming thermonuclear emission.[19] The charge-exchange spectra[20] appear Maxwellian out to energies of approximately $10T_d$. Further confirmation of the thermonuclear origin of the emission comes from collimated neutron spectral measurements, which indicate no nonthermal broadening or shifting of the 2.45 MeV neutron emission line during $H^0 \rightarrow D^+$ neutral beam injection on PLT,[21] ^{3}He-minority ICRH on PLT,[22] or Ohmic heating on TFTR[23] or PLT.

III. DATA

Typical neutron sawtooth behavior during ^{3}He-minority ICRH in PLT is shown in Fig. 1(a). No significant change ($< 1\%$) in neutron emission accompanies the large, sudden drop in electron temperature (typically 25% in 50 μsec) seen at the sawtooth crash (Fig. 2). Subsequently, the neutron emission drops on a slower time scale (about a 10% reduction in approximately 0.5 msec) and then declines an additional $\sim 5\%$ at a still slower rate to an absolute minimum in about 5 msec. This change in the rate of decay of the emission is seen more clearly by plotting the slope of the neutron signal (Fig. 3). The overall reduction in emission at this sawtooth was $\Delta I_n/I_n = 18\%$. After the minimum, the emission increases until the subsequent sawtooth occurs approximately 15 msec later. The ion temperature was $T_d \simeq 3$ keV in this discharge.

Neutron sawtooth behavior during Ohmic heating in TFTR is illustrated in Fig. 1(b) from a plasma fueled by two pellets ($T_d \simeq 2.0$ keV). The drop in neutron emission ($\Delta I_n/I_n = 22\%$) is comparable to that observed in PLT, but the signal takes approximately four times longer to reach its minimum. The initial rate of decay of the emission is comparable for the two devices, even though the electron temperature drop occurs more slowly (100 μsec) in TFTR than in PLT. In both machines, there appears to be a discontin-

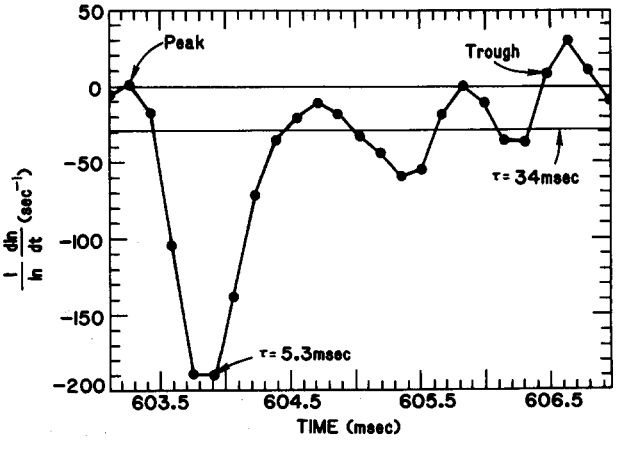

FIG. 3. Time derivative of the neutron rate shown in Fig. 1(a), showing a discontinuity between 450 and 650 μsec after the beginning of the sawtooth. The decay rate prior to this time (mixing phase) is approximately 5 msec, compared with approximately 34 msec afterward (equilibration and transport phases). The points shown are the numerical derivative of a spline fit to a ten-point average of the 100 kHz data. The amplifier response is about an order of magnitude faster than the fast drop rate.

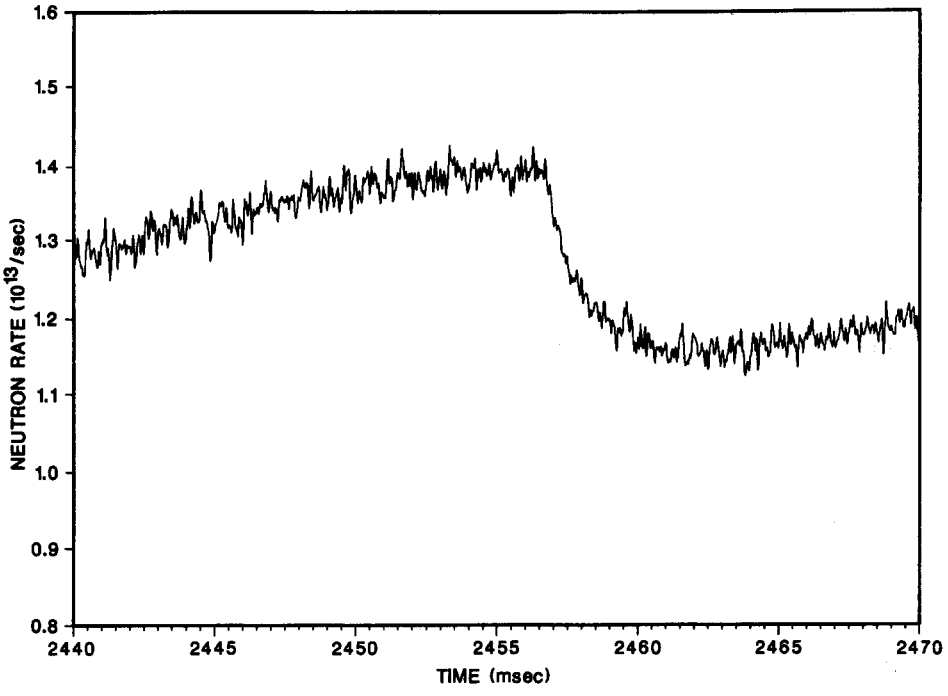

FIG. 4. Neutron sawtooth during $H^0 \rightarrow D^+$ beam injection in an H-mode plasma in DIII-D: $I_p = 1.25$ MA, $B_t = 2.1$ T, $\bar{n}_e = 8.0 \times 10^{13}$ cm^{-3}, $P_b \simeq 7$ MW.

uity in the rate of decay of the emission approximately 0.5 msec after the sawtooth. The sawtooth period in this TFTR plasma (not shown) is approximately eight times longer than in the PLT plasma.

A neutron sawtooth during the H mode in DIII-D is shown in Fig. 4. The initial rate of decay of the neutron emission is similar to that observed on PLT and TFTR. The signal reaches its minimum value faster than a typical TFTR sawtooth but slower than a typical PLT sawtooth. The sawtooth period (approximately 50 msec) is also intermediate between PLT and TFTR. The overall drop in emission was $\Delta I_n / I_n = 17\%$ at this sawtooth in a plasma with $T_d \simeq 1.3$ keV. Typical sawtooth behavior in the three devices is compiled in Table I.

Several features of the initial drop in emission are noteworthy. One striking feature of the data is that the initial rate of decay is comparable on the three devices (Table I). In contrast, the electron crash time, the overall neutron decay time, and the sawtooth period differ greatly between machines. A second feature is that, in some plasmas, little drop in neutron emission occurs on the time scale of the electron sawtooth. This is seen most clearly on PLT (Fig. 2), where the electron sawtooth is fastest, but is also observed at some sawteeth on DIII-D (Fig. 5). A third feature of the initial decay is its variability. The decay rate at nominally similar sawteeth in the same plasma varies by nearly a factor of 2 under some DIII-D and TFTR conditions. In light of this variability, it seems unlikely that the initial rate of decay depends on global discharge parameters in a simple manner. Indeed, little correlation with $\bar{n}_e$, T_e, or T_i is observed. On PLT, the magnitude of the initial drop correlated with the fractional change in electron temperature and with the sawtooth radius; this correlation was not observed in DIII-D, however. In summary, the initial decay of the emission is (i) comparable in different tokamaks, (ii) sometimes slower than the electron sawtooth, and (iii) variable in its dependence on global parameters.

After the initial rapid decay, the emission falls gradually to a minimum. For PLT, the peak-to-trough sawtooth time, t_{p-t}, scales with the magnitude of the sawtooth period (Fig.

TABLE I. Thermonuclear neutron sawtooth behavior.

Tokamak	a(cm)	R(cm)	Electron crash (msec)	Rapid drop Rate^{-1} (msec)[a]	Rapid drop Magnitude[b]	Total drop Duration (msec)[c]	Total drop Magnitude[d]	Sawtooth period (msec)
PLT	40	132	~0.03	0.3–0.7	~60%	~5	~15%	~15
DIII-D	67	167	~0.10	0.3–1.5	~20%	~7	~43%	~30
TFTR	80	255	~0.30	0.3–1.2	~30%	~20	~32%	~130

[a] $\Delta I_n / (dI_n/dt)$ during rapid drop in emission.
[b] Fraction of total drop ΔI_n.
[c] t_{p-t}.
[d] $\Delta I_n / I_n$ for $\Delta T_e / T_e = 20\%$.

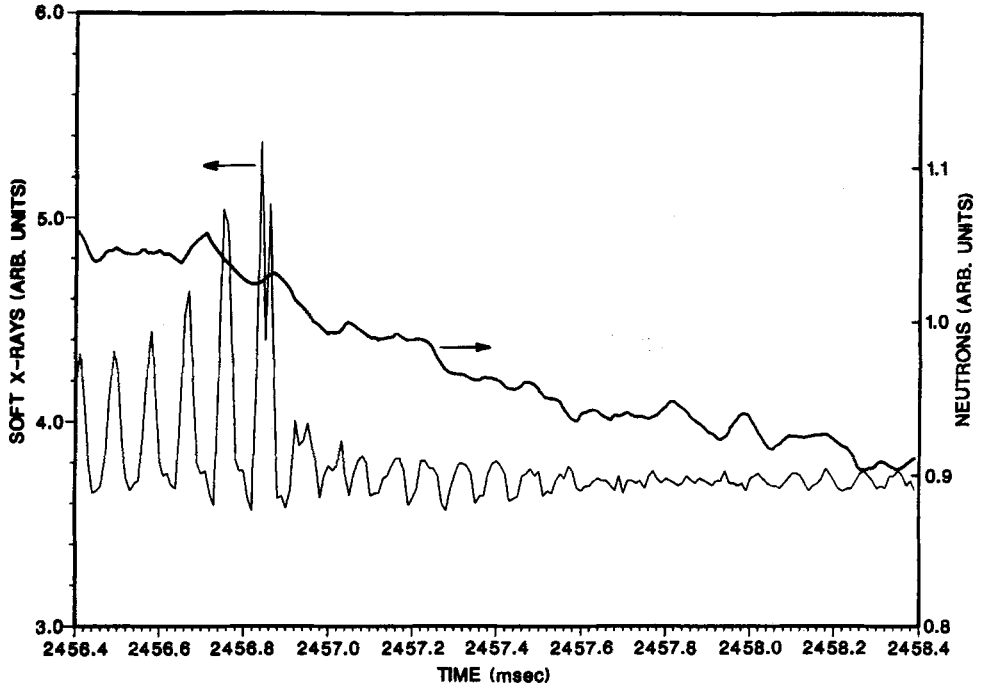

FIG. 5. Central soft x-ray and neutron signals during the sawtooth shown in Fig. 4.

6), which also scales with the magnitude of the neutron drop $\Delta I_n/I_n$, but this scaling was not observed on TFTR. No direct correlation with heating method or power, electron temperature or density, central ion temperature, toroidal magnetic field, or plasma current was observed in any device. A comparison of t_{p-t} for different devices (Fig. 7) indicates that the peak-to-trough time scales approximately with machine minor radius to the second power (a^2), suggesting a dependence on transport processes. A quantitative comparison of the PLT data with a transport model is given in Sec. IV D.

For a given discharge condition, the drop in neutron emission from peak-to-trough $\Delta I_n/I_n$ scales approximately linearly with the drop in electron temperature $\Delta T_e/T_e$ in all three tokamaks. This is illustrated in Fig. 8 for Ohmically

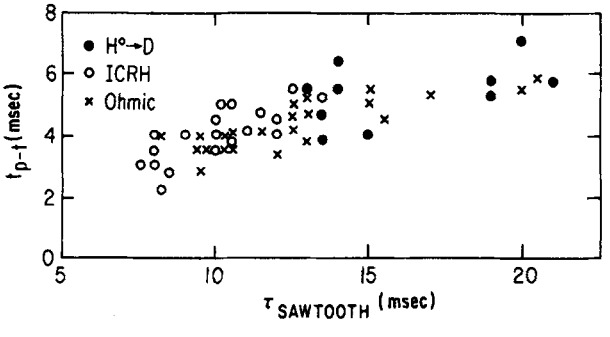

FIG. 6. Peak-to-trough decay time versus sawtooth period for PLT plasmas with various types of heating. The drop in neutron emission $\Delta I_n/I_n$, also scales with the sawtooth period.

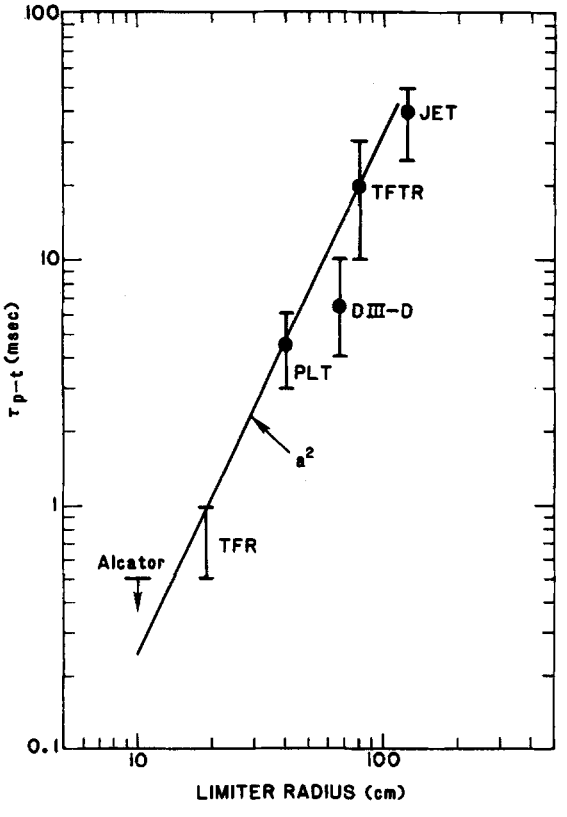

FIG. 7. Peak-to-trough decay time τ_{p-t} versus machine minor radius a on Alcator A,[2] TFR,[3] PLT, DIII-D, TFTR, and JET.[4] The line is an a^2 scaling, suggesting a dependence on radial transport. For Alcator A, the measurement of τ_{p-t} may have been affected by the instrumental resolution. The errors bars for TFR, PLT, DIII-D, and TFTR indicate the range of values observed; for JET, the error bar indicates the variation in a single discharge. In noncircular plasmas, the short axis is used.

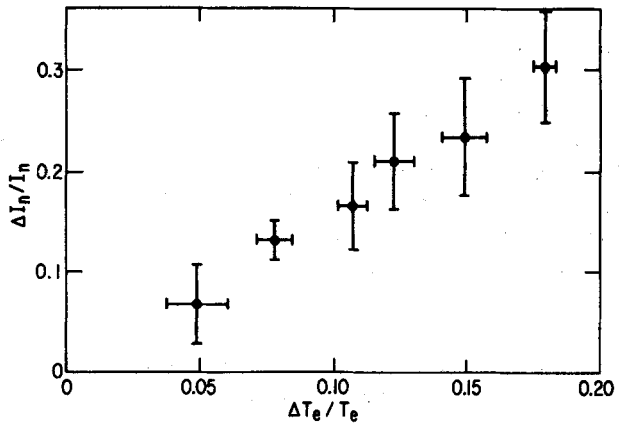

FIG. 8. Fractional drop in neutron emission versus fractional drop in electron temperature for Ohmic TFTR discharges. The points are averages over many sawteeth.

heated TFTR plasmas. For these plasmas with $T_d \simeq 2.0$ keV, $\Delta I_n/I_n \simeq 1.6\Delta T_e/T_e$. In ICRH PLT plasmas a linear correlation is also observed but, in these hotter plasmas ($T_d \simeq 3.0$ keV) the coefficient of proportionality is smaller ($\Delta I_n/I_n \simeq 0.6\Delta T_e/T_e$). In $H^0 \rightarrow D^+$, DIII-D H-mode plasmas, the ion temperature is lower than in TFTR ($T_d \simeq 1.3$ keV) and the scaling of $\Delta I_n/I_n$ with $\Delta T_e/T_e$ is stronger ($\Delta I_n/I_n \simeq 2.1\Delta T_e/T_e$). Presumably, some of the variation in the coefficient of proportionality is due to the temperature dependence of the fusion reactivity. For $\overline{\sigma v} \propto T_d^c$, where c is a function of temperature (and assuming that the ion temperature sawtooth is responsible for most of the drop in neutron emission), the expected reduction in neutron emission is roughly $\Delta I_n/I_n \simeq c\,\Delta T_d/T_d$. This implies that $\Delta T_d/T_d \simeq 0.4\Delta T_e/T_e$ in DIII-D and TFTR but $\Delta T_d/T_d \simeq 0.2\Delta T_e/T_e$ in PLT. Thus the temperature dependence of the reactivity accounts for some of the variation in scaling between devices but cannot fully explain the differences. One possibility is that the drop in neutron emission is smaller on PLT because the sawtooth period is shorter so that the plasma begins to reheat prior to termination of the transport phase. On PLT, the initial drop (δI_n after approximately 0.5 msec) is a larger fraction of the total drop ($\simeq \frac{2}{3}$) than on TFTR ($\sim \frac{1}{3}$) or on DIII-D ($\simeq \frac{1}{4}$) (Table I).

IV. ANALYSIS

The behavior of the thermonuclear neutron emission at a sawtooth suggests that several physical processes are responsible for the observed time evolution. In this section, we consider four phases in the evolution of the ion distribution function in an attempt to explain our results. The phases are illustrated in Fig. 9. In the first phase [Fig. 9(a), Sec. IV A], the ion density flattens to preserve quasineutrality when the electron density collapses. At the end of this phase, the deuterium number density is uniform within the mixing radius, but the velocity distribution is not. This phase results in little change in neutron emission. In the second phase [Fig. 9(b), Sec. IV B], the velocity distribution becomes homogeneous and the emission falls. At the end of this phase, the velocity distribution is not Maxwellian but it is uniform in space. The last two phases run concurrently: the perturbed ion distribution relaxes to a Maxwellian distribution [Fig. 9(c), Sec. IV

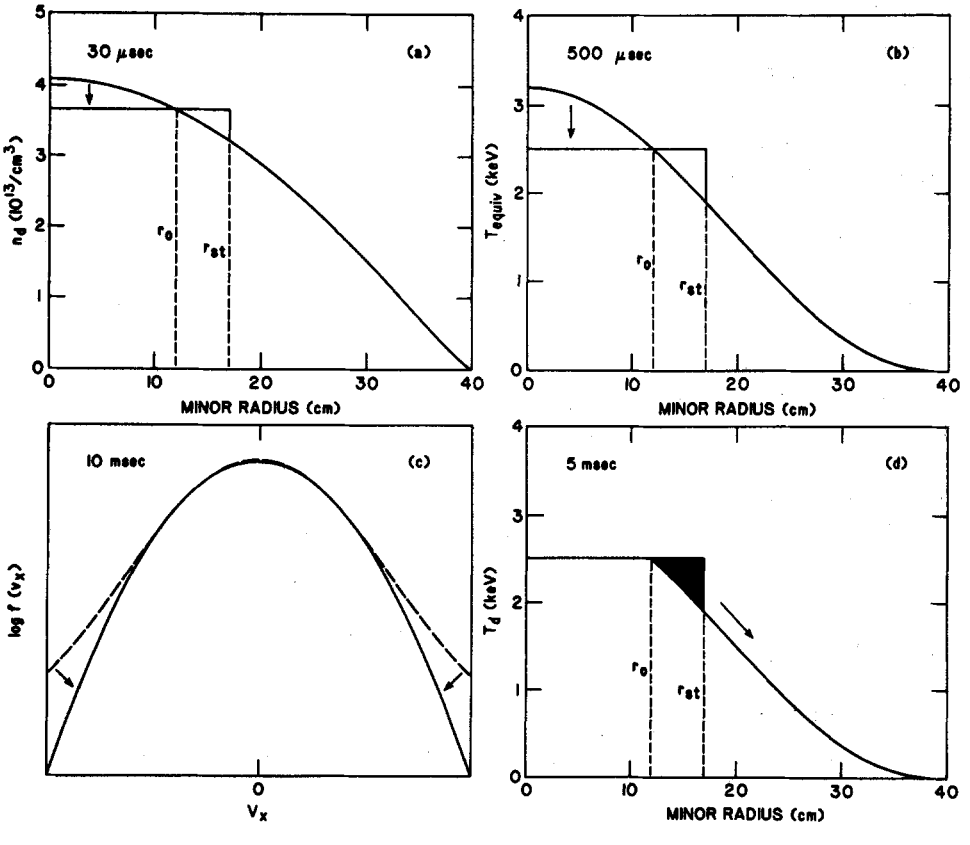

FIG. 9. Four phases of neutron sawtooth crash: (a) crash phase, in which the ion density profile flattens to preserve quasineutrality; (b) mixing phase, in which the ion distribution is homogenized in the sawtooth region; (c) equilibration phase, in which a Maxwellian velocity distribution is reestablished; and (d) thermal transport phase, in which the "shoulder" on the ion temperature profile diffuses away.

C] and an ion heat pulse propagates away from the plasma center as the steep gradient in the ion temperature near the mixing radius diffuses [Fig. 9(d), Sec. IV D]. Both of these processes cause further reduction in the neutron rate. The neutron sawtooth ends when ion heating overcomes the energy loss from thermal conduction and the central deuterium density begins to peak on axis. When the presawtooth conditions are reestablished, the cycle is repeated. In the following four sections, the predicted effect of each of these processes is derived and compared with experiment.

A. Density crash phase

The sawtooth instability has been observed to flatten (or slightly hollow) the electron density on TFR[3] and sawtooth behavior in n_e has been clearly observed on TEXT.[24] The PLT Thomson scattering and TFTR five-channel interferometer[6] measurements are consistent with these observations. Since the plasma is constrained to remain quasineutral, the electron density crash implies a concurrent ion density crash. Measurements on Alcator C[8] indicate that the impurity silicon density is flattened at a sawtooth. While it is possible that the density sawtooth for deuterons could differ from that for impurity ions, observations with $d(^3\mathrm{He},p)\alpha$ proton detectors reported here in low Z_{eff} discharges give direct evidence of deuterium density flattening on the time scale of the electron density sawtooth crash (Appendix B). Previous experiments with d-^{3}He proton detectors on PLT[25] and JET[26] and active charge exchange[27] on PLT suggest that energetic ^{3}He ions and fast deuterons are also redistributed at a sawtooth.

Conceivably, deuterons could gain energy during the crash phase, as was observed during disruptions on LT-3.[28] This would result in an increase in neutron emission. Alternatively, if a significant fraction of hot tail deuterons were lost or redistributed over much of the plasma, the emission would be expected to drop. Experimentally on PLT, little change ($<1\%$) is observed in the neutron emission on the time scale of the electron temperature sawtooth crash (Fig. 2). Typically, a 4% drop in I_n is observed in DIII-D and TFTR during the electron crash phase, but some of this drop may be associated with the mixing phase, since the electron sawtooth is slower than on PLT. The frequency response of the neutron system on PLT is sufficient to record fluctuations three to four times faster than those observed in Fig. 2, so it appears that the neutron rate is actually quite insensitive to the electron redistribution. Nevertheless, $d(^3\mathrm{He},p)\alpha$ proton measurements show that the deuterium density profile *is* redistributed on the fast ($30\,\mu$sec) time scale (Appendix B). As shown in Sec. IV B, if the ions were uniformly mixed at the electron sawtooth, a reduction of approximately 5% in neutron emission is expected. Conceivably, some liberated magnetic energy could heat the ions, thereby masking the drop associated with ion mixing. This explanation seems unlikely, however, since the neutron emission does drop to the expected level on a 1 msec time scale and it seems unlikely that this liberated energy would be so rapidly lost. How then can the density flatten without the ions mixing? One possibility is that the ion density flattening is accomplished locally through small ($\lesssim 0.2$ cm) displacements of bulk-plasma volume elements (Fig. 10); such a redistribution would have a small effect on the volume-integrated fusion emission. This is analogous to the way that a mound of viscous jelly would flatten under the influence of gravity; little real particle mixing would be involved. A second possibility is that the deuterons collapse like a mound of pebbles: in this scenario, the density after the crash is fairly uniform but fine-scale variations in temperature still exist. A third possibility is that the warm, fusion-producing ions do not mix as rapidly as the thermal ions.

In summary, the relatively small drop in neutron emission on the time scale of the PLT sawtooth suggests that (i) little energy is lost or gained by the ions at the crash and (ii) the velocity distribution function $f(\mathbf{r},\mathbf{v})$ retains some dependence on $\mathbf{r}$ after the crash. In the next phase, the "mixing phase," this spatial structure is lost and the velocity distribution becomes uniform.

B. Mixing phase

A drop in neutron emission is expected if the ion temperature and density are flattened at a sawtooth. In this section, we calculate the expected reduction in emission for a uniform redistribution within the mixing radius using a heu-

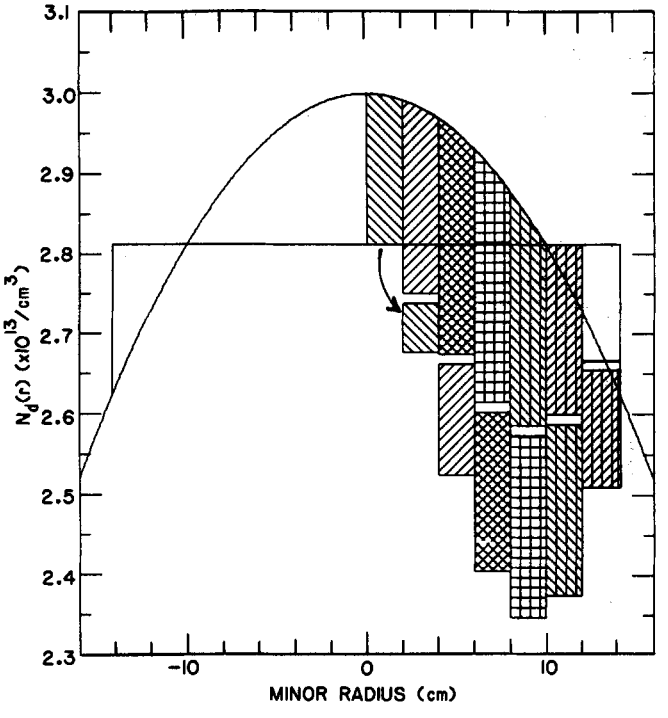

FIG. 10. Local redistribution of deuterons without significant mixing, implying little change in fusion neutron emission. Each shaded region moves outward by one radial shell (to the corresponding shaded region) at the sawtooth. At the inversion radius ($r = 10$ cm in the diagram), an integrated density corresponding to the entire excess from the central portion of the pre-crash profile is displaced by one radial step. The minimum radial step size consistent with local density redistribution is thus given by the interval Δr for which a shell at the inversion radius contains a total number of ions equal to this ion excess. For a parabolic density profile and an inversion radius at $a/4$, $\Delta r = a/240$ or 0.17 cm on PLT. A flattening of the ion density occurring through radial displacements of this size should show little ($<1\%$) change in neutron emission.

ristic analysis (Sec. IV B 1). Next, the predicted drop is calculated numerically (Sec. IV B 2) and compared with experiment (Sec. IV B 3).

1. Heuristic analysis

The $d(d,n)$ ^{3}He neutron emission rate in a deuterium plasma is

$$I_n = \int \frac{1}{2} n_d^2 \langle \sigma v \rangle_{d,n} \, dV, \tag{1}$$

where n_d is the deuterium density and $\langle \sigma v \rangle_{d,n}$ is the $d(d,n)$ ^{3}He fusion reactivity

$$\langle \sigma v \rangle_{d,n} \equiv \int\int f_1(\mathbf{v}_1) f_2(\mathbf{v}_2) \sigma v \, d\mathbf{v}_1 \, d\mathbf{v}_2. \tag{2}$$

Here, $\mathbf{v}_1$ and $\mathbf{v}_2$ are the velocities of the reacting particles, $v = |\mathbf{v}_1 - \mathbf{v}_2|$, and σ is the $d(d,n)$ ^{3}He fusion cross section. For a Maxwellian plasma of temperature T_d, this equation can be rewritten in terms of the center-of-mass velocity $V_{\rm cm}$ and relative velocity v[29]:

$$\langle \sigma v \rangle_{d,n} = \left[\left(\frac{m_d}{4\pi T_d} \right)^{3/2} \int \exp\left(-\frac{m_d v^2}{4T_d} \right) \sigma(v) v \, d\mathbf{v} \right] \times \left[\left(\frac{m_d}{\pi T_d} \right)^{3/2} \int \exp\left(-\frac{m_d V_{\rm cm}^2}{T_d} \right) dV_{\rm cm} \right].$$

Using the Gamow cross section of form $\sigma(v) = (C_1/v^2)\exp(-C_0/v)$,[30] the integrand of the relative velocity integral has a sharp maximum for $(C_0 v_{\rm th}^2)^{-1/3} v = 1$, with $C_0 = 1.482 \times 10^9$ cm/sec. This corresponds to $v/v_{\rm th} = 3.63 T_d^{-1/6}$, for T_d in keV. The integrand of the center-of-mass velocity integral is much broader, giving a most probable value of $V_{\rm cm}/v_{\rm th}$ at $1/\sqrt{2}$ and an average value at $\sqrt{2/\pi}$. Thus the ratio of relative to center-of-mass velocities of the deuterons in a typical fusion reaction is $v/V_{\rm cm} \simeq 4.3$ for $T_d = 3$ keV, which implies that the most probable reaction is one between ions in the tail of the distribution directed in nearly opposite directions. A typical reacting ion has energy

$$E_h = \frac{1}{2} m_d v_1^2 \simeq \frac{1}{2} m_d \left[V_{\rm cm}^2 + \left(\frac{v}{2} \right)^2 \right] \simeq \left[\frac{1}{2} + \frac{1}{4} \left(\frac{C_0}{v_{\rm th}} \right)^{2/3} \right] T_d, \tag{3}$$

which implies $E_h \simeq 3T_d$ for ion temperatures near 3 keV.

The effect on the neutron emission of deuterium mixing can now be treated with a simple heuristic model. In this model, the deuterium particle and velocity distributions are made uniform inside of a mixing radius $r_{\rm st}$ at the sawtooth crash. In the mixing region, $I_n \simeq k \int_0^{r_{\rm st}} n_h^2 r \, dr$, where n_h is the density of hot ions with $E_h \simeq 3T_{d0}$ that produce most of the fusion reactions, and k is a constant proportional to the $d(d,n)$ ^{3}He fusion reactivity. Prior to the sawtooth crash, $n_h \equiv \bar{n}_h + \delta n_h$, where $\bar{n}_h$ is the post-crash density and $\int_0^{r_{\rm st}} \delta n_h r \, dr = 0$ by particle conservation. After mixing, the emission in the sawtooth region is

$$I_{a,r<r_{\rm st}} = k \int_0^{r_{\rm st}} \bar{n}_h^2 r \, dr, \tag{4}$$

while beforehand, the emission in the same region is

$$I_{b,r<r_{\rm st}} = k \int_0^{r_{\rm st}} (\bar{n}_h + \delta n_h)^2 r \, dr = I_{a,r<r_{\rm st}} + k \int_0^{r_{\rm st}} (\delta n_h)^2 r \, dr,$$

invoking particle conservation and Eq. (4) above. The ratio of the neutron rates before and after the crash is

$$\frac{I_b}{I_a} = \frac{I_{b,r<r_{\rm st}} + I_{r>r_{\rm st}}}{I_{a,r<r_{\rm st}} + I_{r>r_{\rm st}}} = 1 + \frac{k \int_0^{r_{\rm st}} (\delta n_h)^2 r \, dr}{I_a}. \tag{5}$$

Equation (5) implies that, if particles are conserved and velocities unchanged, the neutron emission must fall through ion mixing since $I_b/I_a > 1$ for all $\delta n_h \neq 0$. In particular, since most of the fusion reactions occur in the sawtooth region,

$$\frac{I_b}{I_a} - 1 \lesssim \frac{\left[k \int_0^{r_{\rm st}} (\delta n_h)^2 r \, dr \right]}{I_{a,r<r_{\rm st}}} = \frac{2}{r_{\rm st}^2} \int_0^{r_{\rm st}} \left(1 - \frac{n_h(r)}{\bar{n}_h} \right)^2 r \, dr. \tag{6}$$

The density profile of the hot deuterium is estimated assuming a temperature profile of the form $T_d(r) = T_{d0}[1 - (r/a)^2]^{\alpha_T}$. A 1-D Maxwellian velocity distribution has

$$n_h(r) = -\frac{n_d(r)}{\sqrt{\pi E_h T_d(r)}} \exp\left(-\frac{E_h}{T_d(r)} \right) dE \simeq n_{h0} \exp\left(-\frac{kr^2}{r_{\rm st}^2} \right), \quad \text{where } k = \frac{\alpha_T E_h r_{\rm st}^2}{T_{d0} a^2}, \tag{7}$$

and E_h is the energy of the deuterons responsible for most of the fusion emission [Eq. (3)]. After mixing, this distribution is flattened to a constant value $\bar{n}_h$, where, for particle conservation,

$$\pi r_{\rm st}^2 \bar{n}_h = 2\pi \int_0^{r_{\rm st}} n_h(r) r \, dr \Rightarrow \bar{n}_h \simeq (n_{h0}/k)(1 - e^{-k}). \tag{8}$$

With this hot-ion density profile, Eq. (6) gives

$$\frac{I_b}{I_a} - 1 \lesssim \frac{2}{r_{\rm st}^2} \int_0^{r_{\rm st}} \left(1 - \frac{k e^{-kr^2/r_{\rm st}^2}}{1 - e^{-k}} \right)^2 r \, dr = \frac{k}{2} \frac{(1 - e^{-2k})}{(1 - e^{-k})^2} - 1 \simeq \frac{k^2}{12}.$$

Thus the final expression for the magnitude of the drop in neutron emission due to ion mixing is

$$\frac{I_b}{I_a} - 1 \lesssim \frac{1}{12} \alpha_T^2 \left(\frac{E_h}{T_{d0}} \right)^2 \left(\frac{r_{\rm st}}{a} \right)^4 = \mathcal{O}(10\%). \tag{9}$$

2. Numerical analysis

The exact prediction of the mixing model for the magnitude of the fast drop in neutron emission at the sawtooth is evaluated numerically by performing the full six-dimensional velocity space integral [Eq. (2)] for the reactivity, using the mixed deuterium distribution. The distribution function is obtained by homogenizing the pre-crash spatial dependence of $f(r,v)$ in the mixing region:

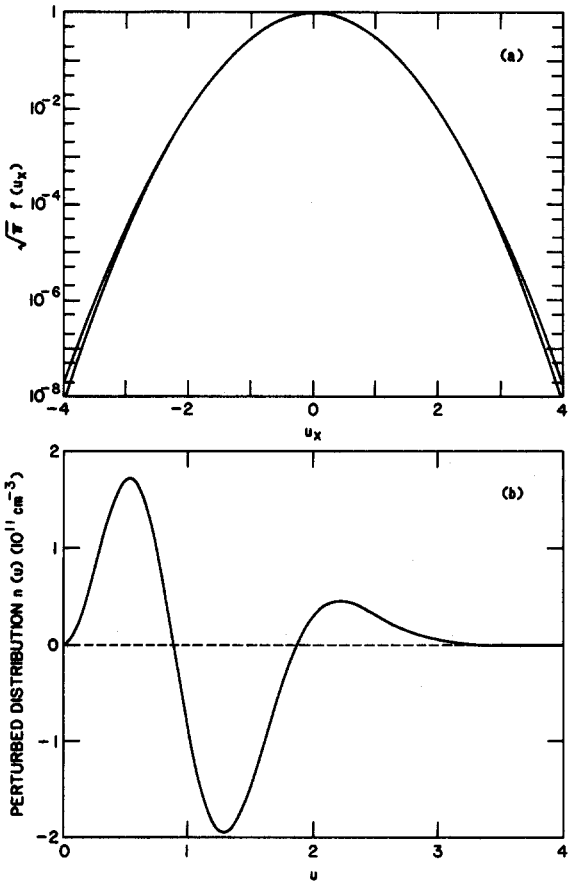

FIG. 11. Distribution function after mixing phase. (a) Post-mixing deuterium distribution function given by Eq. (10) for a plasma with $n_d = 3\times10^{13}(1-r^2/a^2)^{1.2}\,\mathrm{cm}^{-3}$, $T_d = 3(1-r^2/a^2)^{2.5}$ keV, and $r_{st}/a = 0.25$, along with a Maxwellian with the same total energy [the Maxwellian is given by $\pi^{-1/2}\exp(-u_x^2 T_{d0}/\overline{T}_d)$, where $\overline{T}_d$ is the flat-profile temperature given by Eq. (C4) and $u_x = v_x/v_{th}$]. (b) Difference distribution between the perturbed distribution and Maxwellian, with flat-profile density given by Eq. (C3). The integral under this curve is zero, as is required for particle conservation.

$$f_a(v) = \frac{\int_{r<r_{st}} n_d(r) f_M(r,v)\,dV}{\int_{r<r_{st}} n_d(r)\,dV} = \frac{2}{\bar{n}_d r_{st}^2}\left(\frac{m_d}{2\pi}\right)^{3/2}\int_0^{r_{st}} n_d(r)\,T_d^{-3/2}(r) \times\exp\left(-\frac{m_d v^2}{2T_d(r)}\right) r\,dr, \tag{10}$$

where $\bar{n}_d$ is the post-crash deuterium density in the mixing region from Eq. (C3). The resulting distribution function, and its deviation from Maxwellian, is shown in Fig. 11. The surplus at high and low velocities corresponds to excesses of hot and cold particles near $r = 0$ and $r = r_{st}$, respectively. A shortage of particles at the new thermal velocity from the same regions leads to the deficit observed at $v/v_{th} = 1$.

The post-mixing neutron emission from the sawtooth region is then

$$I_{a,r<r_{st}} = \frac{1}{2}\bar{n}_d^2 V\frac{r_{st}^2}{a^2}\int\int f_a(v_1) f_a(v_2)\sigma(v) v\,d\mathbf{v}_1\,d\mathbf{v}_2, \tag{11}$$

where V is the plasma volume. Comparison with the pre-sawtooth neutron rate as determined from Eq. (1) (integrated in the sawtooth region with the Maxwellian reactivity) gives the drop resulting from ion mixing.

The decrease in neutron rate predicted by this model is typically between one-half and two-thirds of the upper limit derived in the heuristic analysis [Eq. (9)], between 2% and 15% of the total neutron rate for typical discharge conditions.

3. Comparison with experiment

With a model of density flattening that includes simultaneous mixing, the drop predicted above would be expected to occur on the same time scale as the electron sawtooth, or approximately 30 μsec on PLT (Sec. IV A). In this scenario, the detector signal would be limited by the frequency response of the photomultiplier amplifier, but would still be three to four times faster than the observed rate (as evidenced by the fastest neutron fluctuations observed with this diagnostic system). Thus it is clear that the ion density flattening and velocity distribution mixing proceed at distinctly different rates. Empirically, it appears that a drop of roughly the predicted magnitude occurs on a longer, 0.5–1.0 msec time scale. Comparing the magnitude of the drop at the end of this phase with the predictions of the mixing model, we find that the actual drop is comparable to that expected theoretically. For the sawtooth events shown in Fig. 1, discharge parameters have been entered in the calculation [Eqs. (10) and (11)] for comparison with the experimental data. The PLT case ($n_{e0} = 5.8\times10^{13}/\mathrm{cm}^3$, $Z_{eff} = 3.0$, density shaping parameter $\alpha_n = 1.4$, sawtooth inversion radius $r_0 = 12$ cm, $T_{i0} = 3.2$ keV, and ion temperature shaping parameter $\alpha_T = 3.0$) has an observed drop of 12.5% in the neutron rate, while the code predicts 12.0%. The TFTR case ($n_{e0} = 5.2\times10^{13}/\mathrm{cm}^3$, $Z_{eff} = 2.2$, $\alpha_n = 0.62$, $r_0 = 23$ cm, $T_{i0} = 2.5$ keV, and $\alpha_T = 2.2$) has an observed drop of 8.3%, with the code giving 4.4%. The PLT inversion radius is inferred from ECE channels separated by 6 cm in major radius and thus has an accuracy of no better than 1 cm in either direction. As the magnitude of the fast drop in neutron rate is roughly proportional to the fourth power of the inversion radius [Eq. (6), along with the relation $r_{st} \simeq \sqrt{2} r_0$, which is derived in Appendix C], the precision of this estimate of $\delta I_n/I_n$ in the mixing phase is only about $\pm$ 30%. The temperature profile exponent ($\alpha_T = 3$) that gives the observed drop is consistent with Doppler-broadening impurity-line measurements[31] of the ion temperature profile during ^{3}He-minority ICRH, but the calculation is somewhat sensitive to small variations in this parameter [$\propto \alpha_T^2$ in the heuristic analysis, Eq. (9)]. Despite the large uncertainty, the results do show that mixing of the deuterium distribution function gives a reduction in neutron emission of the order of that observed, and the data shows that this reduction does not always occur concurrently with the drop in electron temperature, implying that the mixing process for ions is approximately ten times slower than for electrons.

It is possible that the mechanism responsible for ion mixing involves parallel ion motion along the magnetic field

subsequent to field-line reconnection. On PLT, T_e begins increasing again soon after the sawtooth crash, suggesting that closed magnetic surfaces are reestablished on roughly a 30 μsec time scale. Typical ion velocities are sufficiently slow that it is difficult for the ions to mix uniformly this quickly. The observed duration of the mixing phase on PLT (approximately 500 μsec) corresponds to approximately 20 toroidal transits of the ion fluid, or 50 transits of the fast fusion-producing deuterons.

On the other hand, the duration of the mixing phase on TFTR is similar to the duration on PLT at roughly equal temperatures (Table I), despite the fact that a transit around TFTR takes twice as long as on PLT. This suggests that another mechanism may be dominant. Perhaps the rate of decay of the emission is governed by diffusion of a fine-scale structure that exists immediately following the electron crash. Variations in this structure from sawtooth to sawtooth might account for the rather large variations in decay rate observed on TFTR and DIII-D.

In conclusion, the magnitude of the initial drop in neutron emission is consistent with mixing of the ions within approximately 0.5 msec. The time scale for mixing may be determined by the parallel ion velocity, but it could be governed by some other mechanism.

C. Equilibration phase

After the density distribution is mixed, the ions theoretically approach a Maxwellian distribution in an ion–ion equipartition time τ_{ii} (Ref. 32):

$$\tau_{ii} = 4.9\ \text{msec}[T_d(\text{keV})]^{3/2}/Z^* n_e(10^{13}\ \text{cm}^{-3}), \quad (12)$$

where

$$Z^* = \frac{1}{n_e}\sum_f n_f Z_f^2 \left(\frac{2}{A_f}\right)\left(\frac{2A_f}{2+A_f}\right)^{3/2}\frac{\ln \Lambda^{d/f}}{\ln \Lambda^{d/d}}$$

$$\Rightarrow Z^* \simeq \tfrac{4}{5} + \tfrac{1}{5} Z_{\text{eff}} \quad \text{for oxygen impurity.}$$

However, the decay time of the neutron rate due to thermalization is not expected to coincide with τ_{ii} since the ions that produce the fusion reactions are generally more energetic than typical ions. To estimate the actual rate, consider the distribution function created by uniform redistribution of ions within the mixing region (Fig. 11). Describe this distribution by a Maxwellian bulk distribution f_M and a perturbed distribution δf. The neutron emission produced by this distribution consists of a steady rate I_{n0} produced by the bulk Maxwellian ($f_M \cdot f_M$) and a decaying portion δI_n associated with reactions between the perturbed distribution and the bulk ($\delta f \cdot f_M$) and with itself ($\delta f \cdot \delta f$). A numerical investigation shows that the dominant contribution to δI_n is from particles near the peak of the perturbed distribution ($v \simeq 2.3 v_{\text{th}}$) and particles from the Maxwellian bulk distribution with $v \simeq 1.5 v_{\text{th}}$. The reactions are between particles moving in nearly opposite directions, with a relative velocity of about $4 v_{\text{th}}$.

The fast portion of the perturbed distribution, with velocity $v_h \gtrsim 2.3 v_{\text{th}}$, thermalizes more slowly than τ_{ii}^{-1} because of the v^3 dependence of the collision time. The hot ions lose energy at the slower rate τ_{hi}^{-1}, where

$$\tau_{hi} = \frac{1}{3}\sqrt{\frac{2}{\pi}}\, u_h^3 \tau_{ii}\left(\text{erf}(u_h) - \frac{2}{u_h}\text{erf}'(u_h)\right)^{-1}, \quad (13)$$

$$u_h = \frac{v_h}{v_{\text{th}}}.$$

As τ_{hi} represents the decay time constant for the fusion-producing portion of the perturbed distribution, it is a reasonable approximation to the exponential decay time expected for the neutrons [see Eqs. (15) and (16)]. For a total decay δI_n due to velocity-space relaxation,

$$-\frac{\delta I_n}{(dI_n/dt)} \simeq \tau_{hi} \simeq \frac{1}{3}\sqrt{\frac{2}{\pi}}\, u_h^3 \tau_{ii}, \quad (14)$$

giving an expected decay time constant of about $3\tau_{ii}$.

1. Numerical analysis of equilibration

A more quantitative numerical evaluation of the time evolution of the equilibration phase has also been performed to check the heuristic result of Eq. (14). In this study, the post-mixing distribution function $f_a(v)$ calculated from Eq. (10) is allowed to evolve in time through collisional slowing down and parallel diffusion, according to the Fokker–Planck equation. The full six-dimensional velocity-space integral [Eq. (11)] for the neutron rate is calculated at specified time steps to model the actual time evolution of the neutron signal, assuming that the density profile remains flat.

The neutron rate due to the perturbed distribution function δf interacting with a Maxwellian background is

$$I_n = \frac{1}{2}\bar{n}_d^2 V \frac{r_{\text{st}}^2}{a^2}\int\int 2 f_M(v_1)\delta f(v_2)\sigma v\, d^3v_1\, d^3v_2, \quad (15)$$

with the time derivative

$$\frac{dI_n}{dt} = \bar{n}_d^2 V \frac{r_{\text{st}}^2}{a^2}\int\int f_M(v_1)\frac{\partial \delta f(v_2)}{\partial t}\sigma v\, d^3v_1\, d^3v_2. \quad (16)$$

Here $\delta f = f_a - f_M$, where the Maxwellian is taken with the post-crash values $\bar{n}_d$ and $\bar{T}_d$ derived in Sec. IV B, conserving particles and energy in the sawtooth region. The evolution of the perturbed distribution function is given by the Fokker–Planck collision operator. For an isotropic distribution encountering a Maxwellian background plasma with equal deuterium, electron, and impurity temperatures $T_d = T_e = T_{\text{imp}}$,

$$\frac{\partial \delta f}{\partial t} = \sum_{f=e,d,\text{imp}} \frac{m_d}{m_f}\nu_0^{d/f} u \frac{\partial}{\partial u}\left[\left(\delta f + \frac{1}{2u}\frac{\partial \delta f}{\partial u}\right) \times\left\{\text{erf}\left(\sqrt{\frac{m_f}{m_d}}\,u\right) - u\,\text{erf}'\left(\sqrt{\frac{m_f}{m_d}}\,u\right)\right\}\right], \quad (17)$$

where $\nu_0^{d/f}$ is a characteristic collision time

$$\nu_0^{d/f} = 4\pi e_d^2 e_f^2 n_f \ln \Lambda^{d/f}/m_d^2 v_d^3,$$

and u again denotes $v/v_{\text{th},d}$. The terms in the square bracket proportional to δf and its derivative represent collisional slowing down and parallel diffusion of the perturbed distribution, respectively, and obviously sum to zero for a Maxwellian δf.

The time evolution of the distribution function is shown in Fig. 12(a). The distribution decays in about one ion–ion

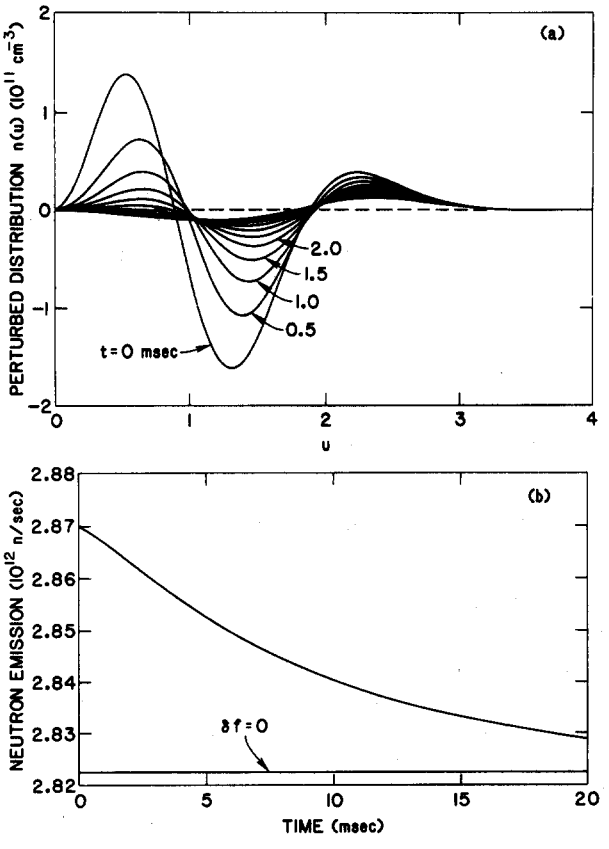

FIG. 12. Thermalization phase. (a) Time evolution of the perturbed distribution function of Fig. 11, using the Fokker–Planck collision operator. The distribution decays in about τ_{ii} (3.5 msec) for values of $u = v/v_{th} < 1.5$, but the hot fusion-producing portion decays much more slowly, in about $3\tau_{ii}$. (b) Corresponding time evolution of the neutron rate, as determined from Eq. (15). The calculated drop is approximately exponential, with a characteristic decay time of 10.2 msec and a relative magnitude of 1.7%.

equipartition time (3.5 msec) for $v < 1.5v_{th}$, but at higher velocities ($v \gtrsim 2.3v_{th}$), the decay time is considerably longer. The result is that the neutron rate I_n decays quite slowly; an approximately exponential decay with a characteristic time constant of 10.2 msec is found for the case shown, where $n_e(r) = 5\times10^{13}(1 - r^2/a^2)^{1.2}/\text{cm}^3$, $T_d(r) = 3(1 - r^2/a^2)^{2.2}$ keV, $r_{st}/a = 0.34$, and $Z_{eff} = 2.5$. This is about three times τ_{ii}, consistent with the heuristic value given by Eq. (14). In addition, it is found that the expected drop for complete relaxation is only a few percent; typically between one-half and two-thirds of the expected drop from the mixing phase. The numerical result for the I_n time evolution is shown in Fig. 12(b), where Eq. (15) has been integrated at each time step for the discharge parameters above. The small contribution to the neutron emission from the region $r > r_{st}$ is unchanged during the disruption and has been omitted from the magnitude of I_n shown in Fig. 12(b). The total drop seen in Fig. 12(b) is only 1.7%, compared with a drop in the mixing phase for these parameters of 2.5%.

The time scale for velocity-space relaxation is thus comparable to the full sawtooth period ($\lesssim$20 msec) on PLT, and the small associated drop in neutron emission (relative to that during the mixing phase) implies that thermalization plays a minor role in the observed time evolution of the PLT neutron sawtooth. In the time required for relaxation of the perturbed distribution, the centrally peaked density and temperature profiles are recovered, and auxiliary heating begins to increase the neutron rate toward its pre-sawtooth level. In TFTR Ohmic discharges [Fig. 1(b)], τ_{ii} is shorter than in high-power ICRH conditions on PLT and the sawtooth period is much longer, so the equilibration phase is allowed to reach completion before the heating phase takes over. In the relatively cold, dense H-mode discharges on DIII-D (Fig. 4), $3\tau_{ii}$ is also shorter than the sawtooth period. In all cases, however, the predicted reduction in emission associated with thermalization is relatively small and the predicted time scale of the reduction is relatively long, so it appears that other processes such as ion transport (Sec. IV D) play a more important role in the evolution of the emission.

D. Transport phase

Both the magnitude and the time evolution of the neutron emission suggest that after the initial rapid drop, transport processes become important. After the ion density and temperature profiles have flattened, a relatively large gradient in plasma density and temperature exists at the edge of the mixing region. The "shoulder" diffuses away on a time scale determined by the local radial ion thermal conductivity and the size and slope of the discontinuity in ion temperature. Particle transport associated with the steep density gradient may also play a role. In this model, while the steep gradient exists, the neutron rate drops due to the loss of energy from the central region of the plasma, where essentially all of the fusion product neutrons are born. In this section, we compute the expected rate of change of the emission during this phase for comparison with PLT data (Sec. IV D 1) and compare the magnitude of the drop with theoretical predictions (Sec. IV D 2).

1. Rate of decay

The $d(d,n)$ ^{3}He reactivity given by the Gamow cross section has a time derivative

$$\frac{1}{\langle\sigma v\rangle}\frac{d\langle\sigma v\rangle}{dt} = \left(\frac{B}{3T_d^{1/3}} - \frac{2}{3}\right)\frac{1}{T_d}\frac{\partial T_d}{\partial t},$$

with $B = 19.87$ for T_d in keV,[30] implying a neutron decay rate due to thermal conduction of

$$\tau_n^{-1} = -\frac{1}{\delta I_n}\frac{dI_n}{dt} = -\frac{1}{\delta I_n}\int \frac{1}{2} n_d^2 \langle\sigma v\rangle \frac{1}{T_d}\frac{\partial T_d}{\partial t}\left(\frac{B}{3T_d^{1/3}} - \frac{2}{3}\right) dV. \quad (18)$$

Here δI_n is the total drop in neutron rate during the transport phase. There is also a reduction in emission associated with particle diffusion but, in this approximation, this term has been neglected.

At the onset of the transport phase, the temperature gradient is negligible everywhere except at the discontinuity at the mixing radius, r_{st}. At this radius, the energy loss due to thermal conduction is

$$4\pi^2 R_0 r_{st}\left[\frac{3}{2} n_d \frac{\partial T_d}{\partial t}\right]\Delta r = \int n_d \chi_d \frac{\partial T_d}{\partial r}\hat{\mathbf{r}}\cdot d\mathbf{A}$$

$$= 4\pi^2 R_0 r_{st} n_d \chi_d \frac{\partial T_d}{\partial r}\frac{\Delta r}{r_{st}}$$

$$\Rightarrow \frac{\partial T_d}{\partial t} = \frac{2\chi_d}{3r_{st}}\frac{\partial T_d}{\partial r}.$$

The surface integral is over two toroidal shells of radii r_{st} and $r_{st} + \Delta r$. Assuming that the only contribution to the volume integral in Eq. (18) is from the discontinuous region,

$$\tau_n^{-1} = -\frac{4\chi_d}{3r_{st}^2}\frac{I_n}{\delta I_n}\left(\frac{B}{3T_d^{1/3}} - \frac{2}{3}\right)\left[\frac{1}{T_d}\frac{\partial T_d}{\partial r}\Delta r\right]_{r_{st}}.$$

The term in square brackets is the change in the temperature profile across the discontinuity:

$$\frac{1}{T_d}\frac{\partial T_d}{\partial r}\Delta r \simeq -\frac{\alpha_T(r_{st}^2 - r_0^2)}{a^2} \simeq -\frac{\alpha_T r_{st}^2}{2a^2},$$

for an ion temperature profile $T_d(r) = T_{d0}(1 - r^2/a^2)^{\alpha_T}$ flattened inside r_{st} to the value $\overline{T}_d \simeq T_{d0}(1 - r_0^2/a^2)^{\alpha_T}$, and invoking Eq. (C5) for r_0. Thus the expected time constant for decay of the neutron emission during this phase is

$$\tau_n \simeq C_1\left(\frac{a^2}{\chi_d \alpha_T}\right)\frac{\delta I_n}{I_n}, \tag{19}$$

where

$$C_1 = \frac{3}{2}\left(\frac{B}{3T_d^{1/3}} - \frac{2}{3}\right)_{r_{st}}^{-1} \simeq 0.4 \quad \text{for } T_d \simeq 3 \text{ keV}.$$

The decay time is thus characterized by the size of the sawtooth region (r_{st}^2), the steepness of the temperature gradient ($\alpha_T r_{st}^2/2a^2$), and the local ion thermal conductivity χ_d at the sawtooth radius.

The peak-to-trough time τ_{p-t} of a sawtooth is dominated by this transport time, since it is long compared to the duration of the mixing phase. Equation (19) suggests that τ_{p-t} should be expected to scale with the square of the minor radius of the device; a plot of observed values of τ_{p-t} for a number of machines is shown in Fig. 7. Assuming a typical ion temperature profile for these machines of $T_d(r) = 2(1 - r^2/a^2)^2$ keV, and $\delta I_n/I_n = 0.1$, the coefficient of the a^2 fit implies an ion thermal diffusivity $\chi_d = 7.5\times 10^3$ cm^2/sec, which is reasonable. Equation (19) represents an estimate of the peak-to-trough time which is actually an upper bound on the expected decay time, since it neglects the effects of particle diffusion. In addition, τ_{p-t} carries a large experimental uncertainty, since the absolute minimum in the neutron emission may simply reflect the time at which the energy gain from auxiliary heating overcomes the energy loss due to thermal conduction, rather than the end of the enhanced conduction phase.

A slight manipulation of Eq. (19) yields

$$-\frac{I_n}{dI_n/dt} \simeq \frac{3}{2}\left(\frac{B}{3T_d^{1/3}} - \frac{2}{3}\right)^{-1}\frac{a^2}{\chi_d \alpha_T}. \tag{20}$$

A plot of the right-hand side of this equation versus the observed neutron decay time constant in the transport phase is shown in Fig. 13 for a series of ICRH discharges on PLT, using Chang–Hinton neoclassical conductivity including impurity effects.[33] The temperature-profile shaping parameter is inferred from the initial reduction in neutron emission, according to the prescriptions discussed below. The value of the neoclassical conductivity is uncertain to $\pm$ 50% due to uncertainties in Z_{eff} and B_θ. Since the derivation of Eq. (20) neglects particle diffusion, the expected drop rate is actually approximately 20% larger (assuming $D_i \simeq \chi_d$). In addition, as the equilibration phase runs concurrently and at a similar rate, the actual drop rate is further enhanced approximately 20%. Thus the data in Fig. 13 are consistent with theory, indicating that thermal conduction probably is the dominant process governing the decay of the neutron emission.

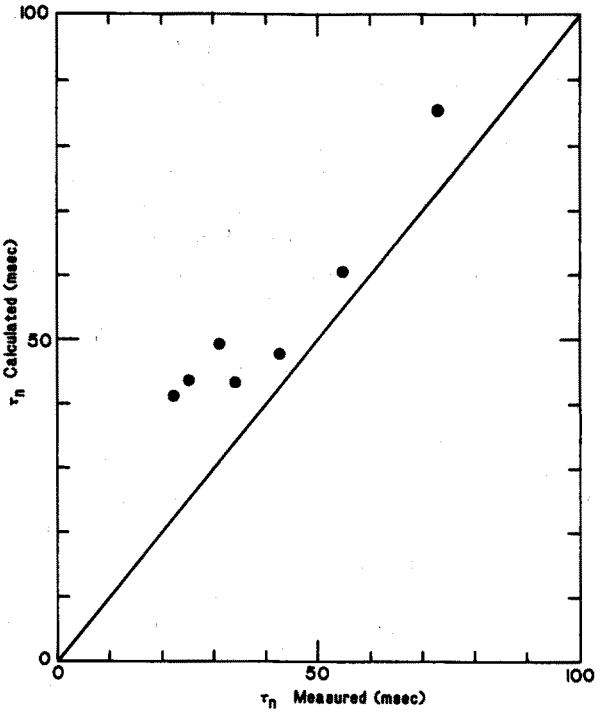

FIG. 13. Right-hand side of Eq. (20) versus the observed neutron emission decay time constant $-I_n/(dI_n/dt)$ during the sawtooth transport phase for a series of ICRH discharges on PLT using Chang–Hinton neoclassical conductivity including impurity effects.[33] The line indicates equality between calculated and experimental drop times. Equation (20) neglects the effects of particle diffusion and velocity-space equilibration.

2. Magnitude of drop

If it is assumed that no ion energy is lost from the mixing radius, the predicted reduction in neutron emission at a sawtooth is much smaller than observed. In this section, we compute the expected drop in neutron emission for various ion temperature profiles and show that the observed drop implies loss of ion energy from the mixing region. Stringer[4] has used a similar mixing model to analyze JET data. With an implicit assumption of energy conservation, he too found that the drop in emission is larger than expected.

We begin by adopting a simple model that we subsequently show is inconsistent with the data. Assume that the ion density and temperature profiles within the mixing radi-

us are flattened and that energy and particles are conserved. Experimentally, two quantities related to the ion temperature profile are measured: the neutron emission I_n and the drop in emission at the sawtooth ΔI_n. Since the deuterium density profile is known fairly accurately from electron density and Z_{eff} measurements and, in any event, the neutron emission is less sensitive to density than to temperature, these two neutron measurements would (if our assumptions were valid) allow us to infer two features of the ion temperature profile. We assume that the functional form of the ion temperature profile is $T_d(r) = T_{d0}(1 - r^2/a^2)^{\alpha_T}$. Then the measurements of I_n and ΔI_n, together with the density measurements and measurement of the mixing radius (inferred from ECE or soft x-ray measurements of the temperature inversion radius), permit unique determination of the central ion temperature T_{d0} and of the peakedness of the temperature profile α_T. Intuitively, for a fixed level of neutron emission, if the drop in emission at the sawtooth is large, then the ion temperature profile must peak strongly on axis. Alternatively, if the initial profile is flat, a sawtooth results in no reduction in emission ($\Delta I_n = 0$).

Quantitative implications of the model are obtained numerically (Appendix C). In Fig. 14(a), we plot the central ion temperature inferred from the drop in neutron emission versus the central ion temperature deduced by a code[34] that uses the neutron emission and the assumption of a neoclassical ion diffusivity profile shape to infer T_{d0}. The temperature inferred from the neutron drop is approximately 25% larger than the values calculated by the analysis code and also exceeds the values measured using Doppler broadened impurity line radiation. For the neutron drop model, the mean temperature peaking parameter for this data set is $\langle \alpha_T \rangle = 3.9$, which is much higher than predicted neoclassically. Recently, the neoclassical χ_i assumption has been shown to be violated on TFTR[35] but not by an amount nearly this large. Even taking into account possible errors and uncertainties in other determinations of the ion temperature, the ion temperature profile inferred by our model is unrealistically peaked. This implies that some ion energy is lost from the mixing region after the sawtooth.

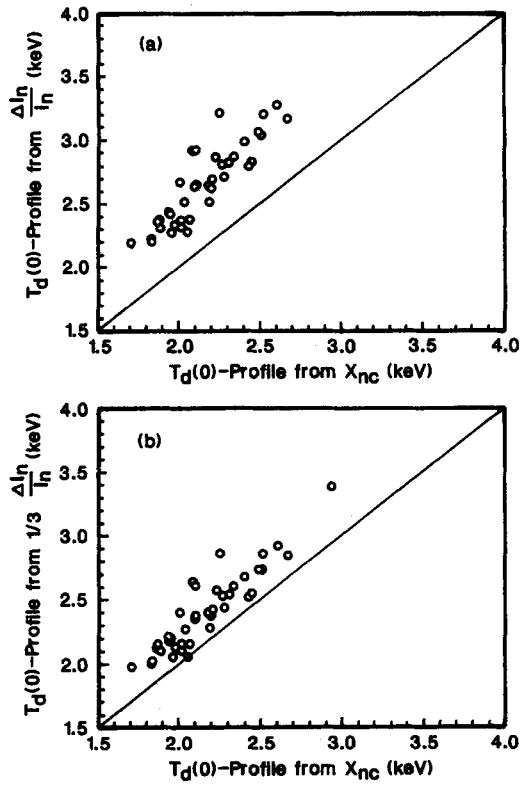

FIG. 14. Implication of the magnitude of the drop in neutron emission ΔI_n. (a) Central ion temperature inferred from the drop in neutron emission versus the central ion temperature calculated by the SNAP[34] analysis code in Ohmic TFTR discharges. The neutron drop temperature is only valid if energy and particles are conserved. The SNAP calculation assumes that the shape of the ion temperature profile is determined by neoclassical diffusivity multiplied by a "neoclassical multiplier." (b) Central ion temperature inferred assuming only one-third of the neutron drop is due to profile flattening versus SNAP temperature.

The time evolution of the neutron emission of TFTR changes after approximately 1 msec [Fig. 1(b)]. At the time that the neutron emission changes slope, the emission has only fallen about $\frac{1}{3}$ of the eventual drop. If we postulate that in this initial period the density and temperature profiles flatten, the computed ion temperature is consistent with the T_i measured by Doppler broadening [Fig. 14(b)]. Using the assumption that only the initial drop is due to profile flattening, the average profile shaping parameter is $\langle \alpha_T \rangle = 2.2$. From the magnitude of the additional reduction in emission, the loss of energy from the mixing region is roughly $\Delta W_d / W_d \simeq 3\%$ for typical parameters. For PLT, using the full drop yields $\langle \alpha_T \rangle = 4.8$, while the analysis gives $\langle \alpha_T \rangle = 2.5$ if the initial neutron drop is used rather than the overall drop.

In conclusion, both the magnitude and the duration of the drop in I_n suggest that energy is lost from the mixing region following the sawtooth.

V. CONCLUSION

At a sawtooth, the neutron emission typically falls about 10% in approximately 0.5 msec, indicating that the hot ions that produce thermonuclear reactions generally take longer to mix than electrons. After the initial rapid drop, the emission falls an additional $\sim 10\%$ in 5–20 msec. Equilibration of the hot ions only accounts for one-fifth of this gradual drop. The data during this phase are consistent with the hypothesis that an ion heat pulse propagates away from the mixing region as the steep gradient in T_i diffuses.

Empirically, the drop in neutron emission $\Delta I_n / I_n$ varies linearly with the drop in central electron temperature $\Delta T_e / T_e$. Estimates of the effect of sawteeth on the thermonuclear emission can be obtained from the scaling $\Delta T_d / T_d \simeq 0.4 \Delta T_e / T_e$.

ACKNOWLEDGMENTS

The support of the PLT, TFTR, and DIII-D staffs is gratefully acknowledged. Gary Estepp and John Evans fabricated the neutron detectors. Data were contributed by M. Bitter, E. Fredrickson, B. Grek, H. Hendel, D. Johnson, K. McGuire, H. Park, A. Ramsey, and G. Taylor for TFTR; by

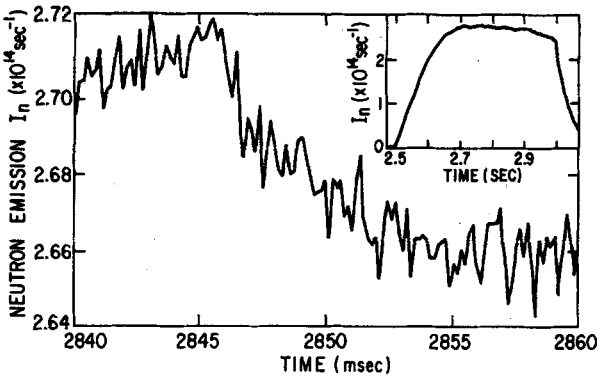

FIG. 15. Sawtooth oscillations in the neutron emission during $D^0 \rightarrow D^+$ neutral beam injection into TFTR from 2.5–3.0 sec. Here, $I_p = 1.8$ MA, $B_t = 4.8$ T, $\bar{n}_e = 3.0 \times 10^{13}$ cm^{-3}, $T_e(0) = 4.4$ keV, $\Delta T_e/T_e = 12\%$, $P_b = 4.3$ MW, $E_b \simeq 76$ keV, coinjection. The magnitude of the total drop is only 3%.

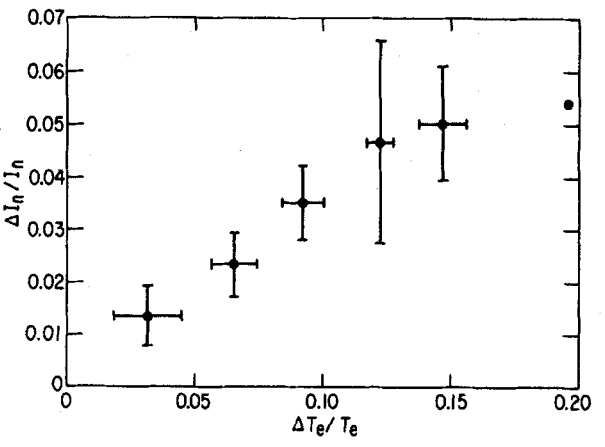

FIG. 16. Fractional change in neutron emission versus fractional change in central electron temperature during $D^0 \rightarrow D^+$ neutral beam injection into TFTR. The points are averages over many sawteeth.

R. Bell, A. Cavallo, P. Colestock, and R. Wilson for PLT; and by T. Carlstrom, J. Lohr, T. Osborne, and R. Snider for DIII-D.

This work was supported by the U. S. Department of Energy under Contracts DE-AC02-76-CHO-3073 and DE-SAC03-84ER51044.

APPENDIX A: EFFECT OF SAWTOOTH ON BEAM–PLASMA NEUTRON EMISSION

To explain the time evolution of the thermonuclear neutron emission, we have postulated several phases of ion response to the sawtooth event (Sec. IV). As a check on the validity of our model, we consider the expected effect of these phases on the neutron emission during $D^0 \rightarrow D^+$ neutral beam injection, when the fusion reactions are beam–plasma in nature. We find that the predictions are consistent with experimental observations.

During $D^0 \rightarrow D^+$ neutral beam injection, the neutron emission is dominated by beam–plasma reactions. Previous work on PLT[12] found that the sawtooth instability causes an approximately 3% drop in neutron emission in approximately 5 msec. On TFTR (Fig. 15), the magnitude of the drop is also only a few percent but the drop is approximately four times slower, varying between 10 and 45 msec. In PLT, the decay was accounted for by the increase in electron drag associated with flattening of the temperature profile.[12] Flattening of the thermal deuterium density also may have played a role.[12] Nominally, the difference in decay time between TFTR and PLT (and DIII-D) is consistent with the increased electron temperature and slowing down time τ_s in TFTR. The decay time in TFTR does not appear to correlate with τ_s, however.

As for thermonuclear neutron sawteeth, the magnitude of the drop in emission $\Delta I_n/I_n$ scales linearly with the amplitude of the electron temperature sawtooth $\Delta T_e/T_e$ (Fig. 16). The magnitude of the drop is five times smaller than in the Ohmic case, however, scaling approximately as $\Delta I_n/I_n \simeq 0.3(\Delta T_e/T_e)$.

For beam–plasma reactions, the neutron emission is approximately

$$I_n \simeq \int n_b n_d \, \overline{\sigma v}_{bd} \, dV, \tag{A1}$$

where n_b is the density of beam ions and $\overline{\sigma v}_{bd}$ is the fusion reactivity for beam–plasma reactions. In steady state, $\overline{\sigma v}_{bd}$ depends principally on the beam injection energy E_b and only weakly on the bulk deuterium temperature T_d. The dependence of the reactivity on ion temperature can be estimated by evaluating the reactivity of a monoenergetic beam in a Maxwellian plasma, $\overline{\sigma v}_{bd} = \int f_d(\mathbf{v}_d) d\mathbf{v}_d \times \sigma v(|\mathbf{v}_b - \mathbf{v}_d|)$. The result is

$$\overline{\sigma v}_{bd} \simeq \sigma v(E_b)\left[1 + (\eta + \tfrac{1}{2})\eta(T_d/E_b)\right], \tag{A2}$$

where $\sigma v(E_b)$ is the reactivity of the monoenergetic beam incident on a cold target and the cross section is assumed to vary approximately as $\sigma v \propto E^\eta$ at $E = E_b$. At $E_b = 80$ keV, $\eta \simeq 2.2$, so, for $T_d \simeq 2$ keV, a 10% reduction in ion temperature only results in a $\lesssim 2\%$ reduction in fusion reactivity.

If beam ions do not gain or lose energy anomalously at a sawtooth, immediately following the sawtooth the fusion reactivity is virtually unchanged since the beam slowing down time τ_s is long compared to the duration of the electron sawtooth. We assume that, prior to the sawtooth, the beam and deuterium densities are $n_b(r) = n_{b0}(1 - r^2/a^2)^{\alpha_b}$ and $n_d(r) = n_{d0}(1 - r^2/a^2)^{\alpha_n}$ and that the beam and deuterium densities flatten at the electron sawtooth. Carrying out a derivation similar to that of Eq. (8), the expected reduction in beam–plasma emission associated with the flattening of the densities is

$$\frac{I_b}{I_a} - 1 \lesssim \frac{1}{12}\alpha_b \alpha_n \left(\frac{r_{st}}{a}\right)^4. \tag{A3}$$

Comparison with Eq. (8) indicates that the beam–plasma drop is smaller than the thermonuclear drop by a factor $\alpha_b \alpha_n / \alpha_T^2 (T_d/E_b)^2 \simeq 0.1$. Thus the expected reduction in beam–plasma neutron emission in the crash and mixing phase is $\lesssim 1\%$. This is in good agreement with experiment, where essentially no change is observed on this time scale.

Following the sawtooth crash, the beam distribution function changes in response to changes in Coulomb drag and the reactivity and beam density become functions of time. The time scale for this transitional period is governed by the slowing down time τ_s. This time scale is several times longer than the equilibration time for hot thermal ions. Since τ_s depends on electron temperature, the flattening of T_e tends to reduce the neutron emissivity within the inversion radius and increase it outside the mixing radius. The beam density is peaked on axis so a net reduction in emission is expected, but the volume-averaged nature of the neutron measurement reduces the predicted reduction to only a fraction of $\Delta T_e/T_e$.[12] Because of the weak dependence of the reactivity on ion temperature [Eq. (A2)], the reduction in T_d associated with the transport phase is expected to have a very small effect on the neutron source strength. Experimentally, the drop in emission does take place on the time scale of τ_s, but the drop time does not correlate with variations in τ_s, perhaps indicating that changes in beam and ion density profiles occur on a similar time scale. The drop in emission is typically 30% of the reduction in electron temperature, in good agreement with theory.

APPENDIX B: EFFECT OF SAWTOOTH ON 15 MeV PROTON EMISSION

During ^{3}He-minority ICRH, the ^{3}He ions are heated to high energies and produce 15 MeV protons in beam–plasma reactions with the thermal deuterium ions. Previous measurements[25] of the volume-integrated proton rate made with a bottom-mounted, collimated surface-barrier detector on PLT showed little or no sawtooth activity, while a side-mounted proton probe did see reductions in d-^{3}He proton emission correlated with drops in central soft x-ray and neutron emission at sawtooth crashes. The interpretation of the difference between the detector signals was that the detection efficiency for the side-mounted probe assembly was strongly peaked near the plasma center, while the bottom-mounted detector integrated over about half of the plasma minor radius, and therefore over the entire sawtooth region.[25] A proton detector on JET[26] with a detection efficiency that is peaked outside of the $d(^3\text{He},p)\alpha$ source region has also shown bursts in signal level at sawtooth crashes, suggesting that energetic ions are expelled from the central region by the sawtooth.

New measurements of the 15 MeV proton emission were made with a detector mounted in the bottom of the PLT vacuum vessel in a geometry similar to that employed previously.[25] These measurements give direct evidence for deuterium density flattening on the time scale of the electron temperature sawtooth. The experimental conditions for these recent measurements are $P_{rf} = 2.5$ MW, ^{3}He-minority concentration $\simeq 5\%$ $\bar{n}_e = 3.7\times10^{13}$ cm^{-3}, and $T_e = 1.5$ keV. Estimates based on Stix's theory[36] suggest that these conditions result in a perpendicular ^{3}He tail temperature of approximately 130 keV. Weighting by the fast-rising fusion cross section, the average energy of the ^{3}He ions responsible for fusion emission is approximately 400 keV for these parameters. Theory[36] and experiment[37] indicate that the ^{3}He ions are accelerated in perpendicular velocity until their orbits become trapped, and then further accelerated until the banana tips migrate outward in major radius to the location of the resonance layer R_{res} (Fig. 17). Particles on these orbits spend most of their time at the turning points, causing a so-called "resonance localization" of the minority, and implying that most of the d-^{3}He fusion occurs at or near the resonance layer. Experimental measurements of the d-^{3}He spatial distribution[38] and anisotropy[39] are consistent with this prediction. As the 400 keV ^{3}He-ion gyrodiameter is approximately 5.4 cm at resonance ($B_t = 29.46$ kG for a 30 MHz ^{3}He-ion cyclotron resonance), the d-^{3}He proton source region is assumed to be the 5 cm of major radius outside of R_{res}. Depending on the relative position of the ICRH resonance layer and sawtooth inversion radius, the emission is observed to decay slowly [Fig. 18(a)], increase gradually [Fig. 18(b)], or increase rapidly (Fig. 19). In Fig. 19, the relative jumps are 5% in 30 μsec, 4% in 30 μsec, and 4% in 50 μsec for the three events shown. These results are evidence for flattening of the deuterium density at a sawtooth.

The effect of density flattening on the d-^{3}He rate is determined in a manner similar to that discussed for the d–d rate in Sec. IV B. The deuterium density is multiplied by the reactivity-weighted ^{3}He-ion density and integrated over the source region before and after a sawtooth. Prior to the sawtooth, the electron temperature profile is assumed to be $T_e(r) = (1 - r^2/a^2)^2$ and the electron, deuterium, and ^{3}He densities are taken to be parabolic, implying a reactivity-weighted ^{3}He-ion density that is roughly parabolic to the second power in the source region, and small outside. The

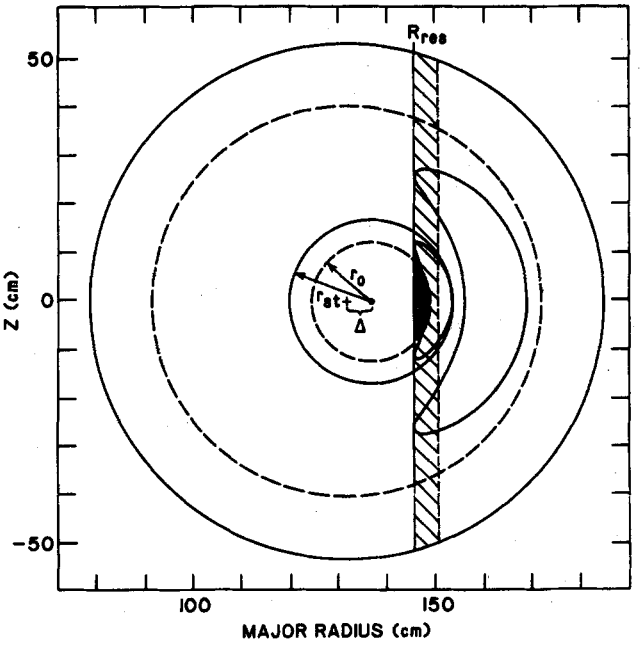

FIG. 17. Guiding-center orbits of 200 keV ions tangent to the resonance layer for 30 MHz rf waves in a 32 kG PLT discharge. The hatched area is the source region for the majority of the $d(^3\text{He},p)\alpha$ proton emission and the doubly hatched region is interior to the sawtooth inversion radius. The relative sizes of the doubly hatched region inside r_0 and the hatched region between r_0 and r_{st} determined the characteristics of the proton sawtooth observed.

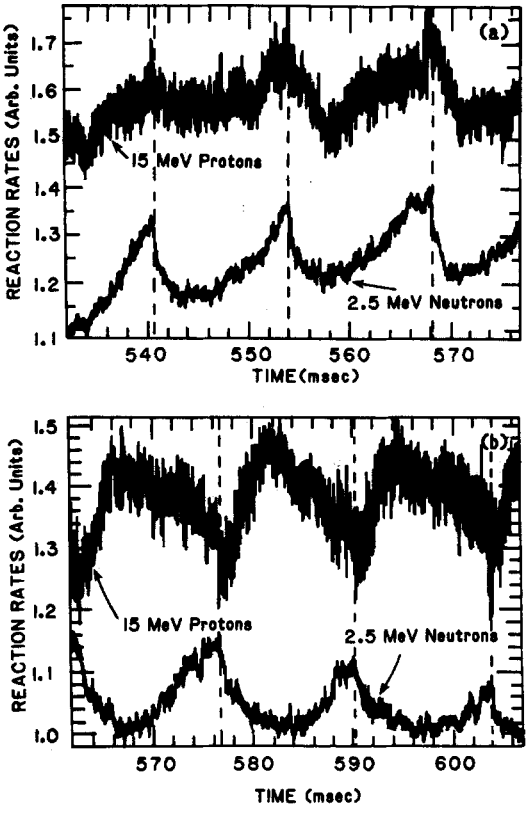

FIG. 18. The 15 MeV proton signal from $d(^3\text{He},p)\alpha$ fusion reactions (top trace), showing that the proton signal can either decrease (a) or increase (b) at a sawtooth: (a) $B_t = 31.8$ kG, $I_p = 530$ kA, $T_{e0} = 2.3$ keV, $\bar{n}_e = 3.7\times10^{13}$ cm^{-3}, $P_{rf} = 2.6$ MW, ^{3}He concentration = 3.6%, $r_{st} = 10$ cm; (b) $B_t = 32.6$ kG, $I_p = 590$ kA, $T_{e0} = 2.2$ keV, $\bar{n}_e = 3.5\times10^{13}$ cm^{-3}, $P_{rf} = 2.4$ MW, ^{3}He concentration = 2.9%, $r_{st} = 9$ cm.

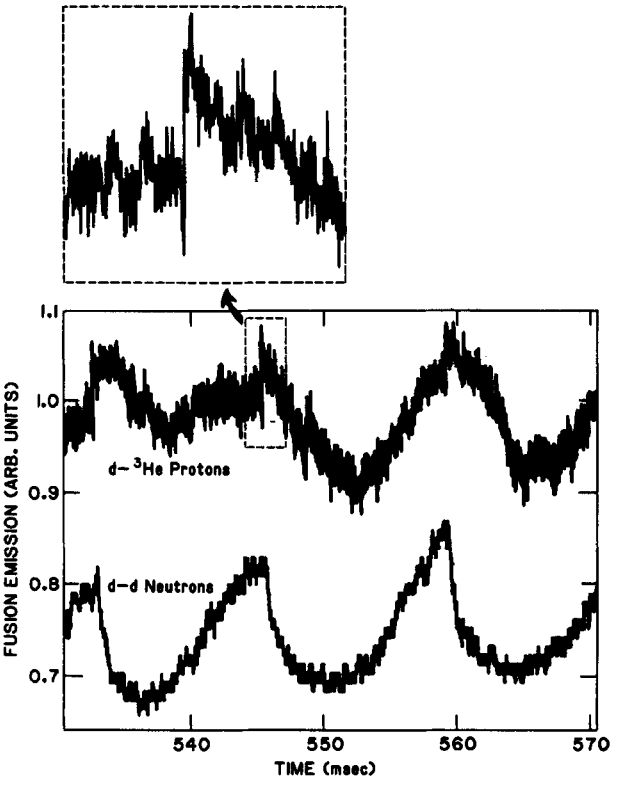

FIG. 19. Sawtooth oscillations in the $d(^3\text{He},p)\alpha$ proton emission for a 2.3 MW ICRH discharge on PLT with a 4% of n_e ^{3}He minority. Discharge parameters are $B_t = 32.6$ kG, $I_p = 570$ kA, $\bar{n}_e = 3.7\times10^{13}$ cm^{-3}, average $T_{e0} = 2.0$ keV, and neutron rate $I_n = 1.4\times10^{12}$/sec, implying an average T_{d0} of about 2.4 keV. Fast increases in proton emission are observed at each neutron sawtooth crash; the jumps are 5% in 30 μsec, 4% in 30 μsec, and 4% in 50 μsec for the three events shown. A detail of the second event is shown for clarity.

actual profile may be steeper, as axial focusing of the rf wave power by the antennas has been neglected. After the sawtooth crash, the deuterium density profile is assumed flattened on the time scale of the electron sawtooth. Depending on the position of the resonance layer with respect to the sawtooth inversion radius, the relative fractions of the source region in which the target density is increased and decreased (the hatched regions in Fig. 17) are determined. Thus it is possible for the proton rate to decline, remain constant, or even increase at the crash, but the magnitude of this change is never more than a few percent (Fig. 20). The change should occur on the time scale of the ion density flattening, or about 30 μsec (not the slower mixing time responsible for the neutron sawtooth crash, since the deuterium is a cold target relative to the energetic ^{3}He). This prediction is consistent with experimental observations (Fig. 19).

The proton sawtooth behavior subsequent to the electron sawtooth is complex. The emission may change due to changes in the energy loss time τ_ϵ, which alters the balance between rf acceleration and collisional deceleration of the tail ions. As the electron density and temperature profiles are flattened at a sawtooth, τ_ϵ decreases for $r < r_0$, thereby decreasing the equilibrium energy of the ^{3}He ions in this region. The opposite is true in the region $r_0 < r < r_{st}$, where both τ_ϵ and the ^{3}He tail temperature increase. Depending on the relative portion of the source volume which falls into these two regions, the net proton emission could be expected to rise or fall. The bottom-mounted PLT detector, which integrates over the full extent of the sawtooth and resonance layer, observed both behaviors at sawtooth events. The proton signal shown in Fig. 18(b) increases about 10% at the neutron sawtooth, suggesting an average increase of about 6% in energy loss time τ_ϵ, which is consistent with the assumed profile shapes given an inversion radius a few cm outside of the resonance layer at the plasma midplane. The toroidal field is again 32.6 kG for this discharge, but the sawtooth region is smaller than that for the discharge shown in Fig. 19, which may explain the difference in time evolution.

APPENDIX C: ION TEMPERATURE PROFILE INFERRED USING A SIMPLE MIXING MODEL

Assume that the ion temperature and density profiles are of functional form $T_d(r) = T_{d0}(1 - r^2/a^2)^{\alpha_T}$ and $n_d(r) = n_{d0}(1 - r^2/a^2)^{\alpha_n}$, respectively, that the profiles are flattened at a sawtooth, and that energy and particles are conserved. Then measurements of neutron emission I_n and reduction in emission ΔI_n, together with measurements of the density profile and mixing radius suffice to determine the central ion temperature T_{d0} and profile shape α_T.

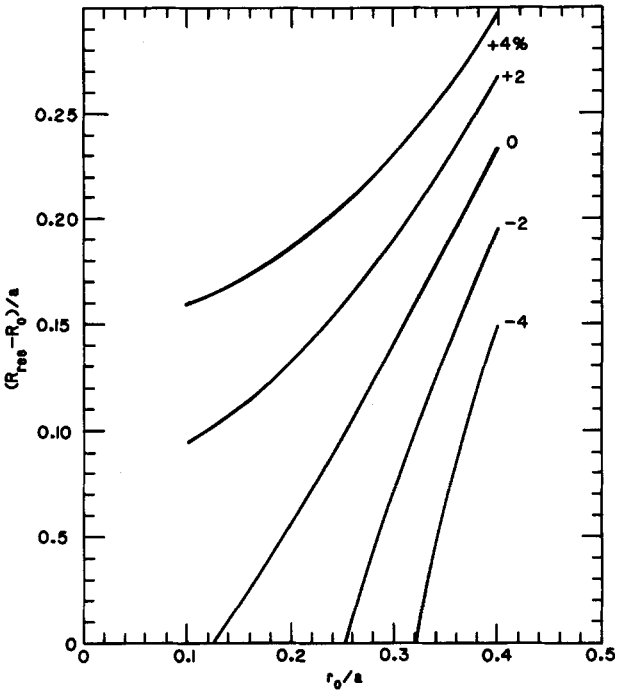

FIG. 20. Expected lines of constant change in the proton emission. The horizontal axis is the sawtooth inversion radius scaled by the plasma minor radius; the vertical axis is the minor radius of the resonance layer at the midplane, also scaled by the plasma minor radius. Calculations are for a source region 5 cm wide bounded by the resonance layer (Fig. 17). The calculated change is never more than 5% for PLT conditions.

Assuming a Gamow form for the fusion cross section,[30] the neutron emission I_n is

$$I_n = \frac{1}{2} A \int n_d^2 T_d^{-2/3} \exp(-BT_d^{-1/3}) dV, \qquad \text{(C1)}$$

where, for the $d(d,n)^3$He reaction, $A = 2.93 \times 10^{-14}$ keV$^{2/3}$ and $B = 19.87$ keV$^{1/3}$. Substitution of the assumed radial profiles for T_d and n_d yields

$$I_n = V n_{d0}^2 A T_{d0}^{-2/3} \int_0^1 x(1-x^2)^C \times \exp[-BT_{d0}^{-1/3}(1-x^2)^{-D}]\, dx,$$

where $x = r/a$, $C = 2\alpha_n - (2\alpha_T/3)$, and $D = \alpha_T/3$. The integral is treated asymptotically using the Laplace method, expanding the integrand around $x = 0$, where the exponential has a maximum:

$$\int \sim \int_0^{\epsilon} x(1 - Cx^2 + \cdots) \times \exp[-BT_{d0}^{-1/3}(1 + Dx^2 + \cdots)]\, dx$$
$$\sim e^{-BT_{d0}^{-1/3}} \int_0^{\infty} (x - Cx^3 + \cdots) \times \left(1 - \frac{D(D+1)}{2} x^4 + \cdots\right) e^{-DBT_{d0}^{-1/3} x^2}\, dx.$$

Carrying out the integration to first order in the small parameter $T_{d0}^{1/3}/B$, we obtain the following result:

$$I_n \sim S_{n0} V / \{1 + 2\alpha_n + [(BT_{d0}^{1/3} - 1)/3]\alpha_T\}, \qquad \text{(C2)}$$

where $S_{n0} = (1/2) n_{d0}^2 A T_{d0}^{-2/3} \exp(-BT_{d0}^{-1/3})$ is the central neutron rate per unit volume. Equation (C2) is particularly illuminating in that it shows the relative effects of the temperature and density profile shapes on the neutron rate. For a 3 keV plasma, the temperature shaping parameter α_T in the denominator is multiplied by 4.25, so the central temperature inferred from the neutron emission is twice as sensitive to temperature-profile shape than to density-profile shape. Although the error in the asymptotic formula is in all cases less than 1.5% of the exact solution from numerical integration of Eq. (C1), we use the exact solution.

A second relation, required to obtain a unique solution for the two-parameter ion temperature profile, is afforded by the magnitude of the drop in neutron emission. By integrating Eq. (C1) numerically in the mixing region to determine the pre-crash neutron rate, and evaluating the post-mixing neutron rate according to a prescribed model, the drop predicted for $\Delta I_n = I_{b,r<r_{st}} - I_{a,r<r_{st}}$ can be compared to the experimentally determined value. In matching the observed data, a unique solution for $T_d(r) = T_{d0}(1 - r^2/a^2)^{\alpha_T}$ is assured, since for any particular value of T_{d0}, δI_n increases with increasing α_T, while I_n decreases. Thus the two curves describing the (α_T, T_{d0}) solution space for the observed neutron rate and its reduction at the sawtooth cross at a single point (Fig. 21).

The deuterium density profile flattens during the mixing phase to the constant $\bar{n}_d$, which conserves particles inside the mixing radius:

$$\pi r_{st}^2 \bar{n}_d = \int_0^{r_{st}} n_d(r) d^2 r$$
$$\Rightarrow \bar{n}_d = n_{d0}\left[1 - (1 - x_{st}^2)^{\alpha_n + 1}\right] / x_{st}^2 (\alpha_n + 1). \qquad \text{(C3)}$$

The post-crash "equivalent temperature" profile is also flattened (the mixed distribution is non-Maxwellian) to a value $\bar{T}_d$ which conserves energy inside the mixing radius:

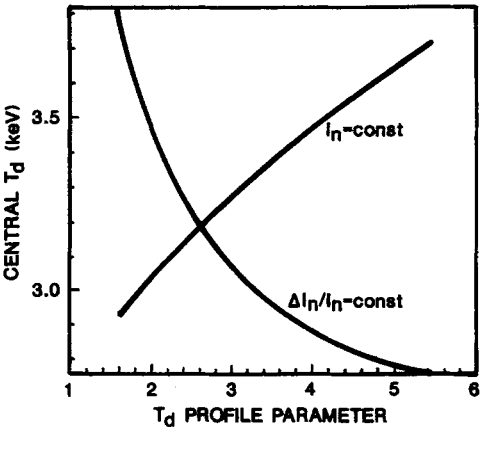

FIG. 21. Lines of constant neutron emission I_n and drop in emission $\Delta I_n/I_n$ in T_{d0} and α_T space for a PLT case. A unique solution for T_{d0} and α_T is assured.

$$\pi r_{st}^2 \bar{n}_d \bar{T}_d = \int_0^{r_{st}} n_d(r) T_d(r) d^2 r \Rightarrow \bar{T}_d = \frac{T_{d0}\left[1-(1-x_{st}^2)^{\alpha_n+\alpha_T+1}\right](\alpha_n+1)}{\left[1-(1-x_{st}^2)^{\alpha_n+1}\right](\alpha_n+\alpha_T+1)}. \quad \text{(C4)}$$

Here $x_{st} = r_{st}/a$. The mixing radius r_{st} was not measured experimentally; instead, the sawtooth size was characterized by the so-called "inversion radius," r_0, at which the response of the soft x-ray emission (corrected for line averaging) and ECE to the sawtooth instability changes sign. Inside of r_0, the electron and ion densities and temperatures drop, accompanied by a drop in x-ray and electron cyclotron emission. Between r_0 and r_{st} the densities and temperatures rise, and the x-ray and electron-cyclotron emissions increase accordingly. The densities remain constant at the inversion radius, so that by definition $\bar{n}_d = n_{d0}(1 - r_0^2/a^2)^{\alpha_n}$. A comparison with Eq. (C3) gives, to first order in r_0/a,

$$r_{st}^2 = 2r_0^2\{1 - [(\alpha_n - 1)/6] r_0^2/a^2\} \Rightarrow r_{st} \simeq \sqrt{2} r_0. \quad \text{(C5)}$$

The relative error introduced by the last approximation is less than 1%, since typically $\alpha_n \sim 1$ and $r_0 < a/3$.

Assuming a Maxwellian distribution exists immediately after the mixing phase, the neutron rate in the mixing region is

$$I_{a,r<r_{st}} = \bar{S}_n V x_{st}^2, \quad \text{(C6)}$$

where $\bar{S}_n = \frac{1}{2}\bar{n}_d^2 A \bar{T}_d^{-2/3} \exp(-B\bar{T}_d^{-1/3})$ is the constant source rate per unit volume throughout the region.

[1] J. Schmidt, G. Bateman, C. Bushnell, J. Citrolo, P. Colestock, D. Ignat, R. Izzo, S. Jardin, L. P. Ku, G. Kuo-Petravic, M. Petravic, C. K. Phillips, N. Pomphrey, D. E. Post, R. B. White, K. M. Young, D. Blackfield, T. Brown, C. Flanagan, Y.-K.M. Peng, T. Shannon, D. Strickler, L. Bromberg, D. Cohn, M. Greenwald, B. Lipschultz, D. B. Montgomery, R. Parker, D. Sigmar, R. Thome, S. Wolfe, W. Houlberg, J. Sheffield, D. Swain, N. Uckan, M. Hughes, C. Paulson, M. Phillips, A. M. M. Todd, G. Kerbel, D. G. Swanson, and F. Puhn, in *Plasma Physics and Controlled Nuclear Fusion Research, 1986* (IAEA, Vienna, 1987), Vol. III, p. 259.

[2] A. Gondhalekar, R. Granetz, D. Gwinn, I. Hutchinson, B. Kusse, E. Marmar, D. Overskei, D. Pappas, R. R. Parker, M. Pickrell, J. Rice, L. Scaturro, J. Schuss, J. West, S. Wolfe, R. Petrasso, R. E. Slusher, and C. M. Surko, in *Plasma Physics and Controlled Nuclear Fusion Research, 1978* (IAEA, Vienna, 1979), Vol. I, p. 199; D. Gwinn and R. Granetz (private communication, 1978).

[3] Equipe TFR, in *Plasma Physics and Controlled Nuclear Fusion Research, 1980* (IAEA, Vienna, 1981), Vol. II, p. 547.

[4] T. E. Stringer (private communication, 1986).

[5] J. M. Adams, O. N. Jarvis, J. Källne, G. Sadler, D. B. Syme, M. T. Swinhoe, N. Watkins, P. van Belle, and K. Verschuur, in *Proceedings of the Fourteenth European Conference on Controlled Fusion and Plasma Physics* (European Physical Society, Budapest, 1987), Vol. II, Part 3, p. 1224.

[6] M. Murakami, V. Arunasalam, J. D. Bell, M. G. Bell, M. Bitter, W. R. Blanchard, F. P. Boody, N. L. Bretz, R. Budny, C. E. Bush, J. D. Callen, J. L. Cecchi, S. A. Cohen, R. J. Colchin, S. K. Comns, J. Coonrod, S. L. Davis, D. L. Dimock, H. F. Dylla, P. C. Efthimion, L. C. Emerson, A. C. England, H. P. Eubank, R. J. Fonck, E. Fredrickson, H. P. Furth, L. R. Grisham, S. von Goeler, R. J. Goldston, B. Grek, R. Groebner, R. J. Hawryluk, H. W. Hendel, K. W. Hill, D. L. Hillis, W. W. Heidbrink, R. Hulse, D. W. Johnson, L. C. Johnson, R. Kaita, R. Kamperschroer, S. M. Kaye, S. J. Kilpatrick, H. Kugel, P. H. LaMarche, R. Little, C. H. Ma, D. M. Manos, D. M. Mansfield, M. P. McCarthy, R. T. McCann, D. C. McCune, K. McGuire, D. M. Meade, S. S. Medley, S. L. Milora, D. R. Mikkelsen, D. Mueller, E. B. Nieschmidt, D. K. Owens, V. K. Pare, H. Park, B. Prichard, A. T. Ramsey, D. A. Rasmussen, M. H. Redi, A. L. Roquemore, P. H. Rutherford, N. R. Sauthoff, J. F. Schivell, G. L. Schmidt, S. D. Scott, S. Sesnic, M. Shimada, J. E. Simpkins, J. C. Sinnis, F. J. Stauffer, J. D. Strachan, B. C. Stratton, G. D. Tait, G. Taylor, C. E. Thomas, H. H. Towner, M. Ulrickson, R. Weiland, J. B. Wilgen, M. Williams, K.-L. Wong, S. Yoshikawa, K. M. Young, M. C. Zarnstorff, and S. J. Zweben, Plasma Phys. Controlled Fusion **28**, 17 (1986).

[7] G. Gammel, R. Kaita, R. Fonck, K. Jaehnig, and E. Powell, Rev. Sci. Instrum. **57**, 1800 (1986).

[8] F. H. Seguin, R. Petrasso, and E. S. Marmar, Phys. Rev. Lett. **51**, 455 (1983).

[9] D. Grove, V. Arunasalam, K. Bol, D. Boyd, N. Bretz, M. Brusati, S. Cohen, D. Dimock, F. Dylla, D. Eames, H. Eubank, B. Fraenkel, J. Girard, R. Hawryluk, E. Hinnov, R. Horton, J. Hosea, H. Hsuan, D. Ignat, F. Jobes, D. Johnson, E. Mazzucato, E. Meservey, N. Sauthoff, J. Schivell, G. Schmidt, R. Smith, F. Stauffer, W. Stodiek, J. Strachan, S. Suckewer, S. von Goeler, and K. Young, in *Plasma Physics and Controlled Nuclear Fusion Research, 1976* (IAEA, Vienna, 1977), Vol. I, p. 21.

[10] J. Luxon, P. Anderson, F. Batty, C. Baxi, G. Bramson, N. Brooks, B. Brown, B. Burley, K. H. Burrell, R. Callis, G. Campbell, T. Carlstrom, A. Colleraine, J. Cummings, L. Davis, J. DeBoo, S. Ejima, R. Evanko, H. Fukumoto, R. Gallix, J. Gillelenad, T. Glad, P. Gohil, A. Gootgeld, R. J. Groebner, S. Hanai, J. Haskovec, E. Heckman, M. Heiberger, F. J. Helton, P. Henline, D. Hill, D. Hoffman, E. Hoffmann, R. Hong, N. Hosogane, C. Hsieh, G. L. Jackson, G. Jahns, G. Janeschitz, E. Johnson, A. Kellman, J. S. Kim, J. Kohli, A. Langhorn, L. Lao, P. Lee, S. Lightner, J. Lohr, M. Mahdavi, M. Mayberry, B. McHarg, T. McKelvey, R. Miller, C. P. Moeller, D. Moore, A. Nerem, P. Noll, T. Ohkawa, N. Ohyabu, T. Osborne, D. Overskei, P. Petersen, T. Petrie, J. Phillips, R. Prater, J. Rawls, E. Reis, D. Remsen, P. Riedy, P. Rock, K. Schaubel, D. Schissel, J. Scoville, R. Seraydarian, M. Shimada, T. Shoji, B. Sleaford, J. Smith, Jr., P. Smith, T. Smith, R. T. Snider, R. D. Stambaugh, R. Stav, H. St. John, R. Stockdale, E. J. Strait, R. Street, T. S. Taylor, J. Tooker, M. Tupper, S. K. Wong, and S. Yamaguchi, in *Plasma Physics and Controlled Nuclear Fusion Research, 1986* (IAEA, Vienna, 1987), Vol. I, p. 159.

[11] P. C. Efthimion, N. Bretz, M. Bell, M. Bitter, W. R. Blanchard, F. Boody, D. Boyd, C. Bush, J. L. Cecchi, J. Coonrod, S. Davis, D. Dimock, H. F. Dylla, S. von Goeler, R. J. Goldston, B. Grek, D. J. Grove, R. J. Hawryluk, H. Hendel, K. W. Hill, R. Hulse, D. Johnson, L. C. Johnson, R. Kaita, S. Kaye, M. Kikuchi, S. Kilpartrick, J. Kiraly, R. Knize, P. LaMarche, R. Little, D. Manos, M. McCarthy, D. McCune, K. McGuire, D. M. Meade, S. S. Medley, D. R. Mikkelsen, D. Mueller, M. Murakami, E. B. Nieschmidt, D. K. Owens, A. T. Ramsey, A. L. Roquemore, N. R. Sauthoff, J. Schivell, J.-L. Schwob, S. Scott, S. Sesnic, J. Sinnis, F. Stauffer, J. D. Strachan, S. Suckewer, G. D. Tait, M. Tavernier, G. Taylor, F. Tenney, H. Towner, M. Ulrickson, K.-L. Wong, A. Wouters, H. Yamada, K. M. Young, and M. Zarnstorff, in *Plasma Physics and Controlled Nuclear Fusion Research, 1984* (IAEA, Vienna, 1985), Vol. I, p. 29.

[12] J. D. Strachan, P. L. Colestock, S. L. Davis, D. Eames, P. C. Efthimion, H. P. Eubank, R. J. Goldston, L. R. Grisham, R. J. Hawryluk, J. C. Hosea, J. Hovey, D. L. Jassby, D. W. Johnson, A. A. Mirin, G. Schilling, R. Stooksberry, L. D. Stewart, and H. H. Towner, Nucl. Fusion **21**, 67 (1981).

[13] W. W. Heidbrink, Rev. Sci. Instrum. **57**, 1769 (1986).

[14] J. D. Strachan, B. Grek, W. Heidbrink, D. Johnson, S. M. Kaye, H. W. Kugel, B. LeBlanc, and K. McGuire, Nucl. Fusion **25**, 863 (1985).

[15] W. W. Heidbrink, K. Bol, D. Buchenauer, R. Fonck, G. Gammel, K. Ida, R. Kaita, S. Kaye, H. Kugel, B. LeBlanc, W. Morris. M. Okabayashi, E. Powell, S. Sesnic, and H. Takahashi, Phys. Rev. Lett. **57**, 835 (1986).

[16] R. Kaita, W. W. Heidbrink, G. W. Hammett, A. A. Chan, A. C. England, H. W. Hendel, S. S. Medley, E. Nieschmidt, A. L. Roquemore, S. D. Scott, J. D. Strachan, G. D. Tait, G. Taylor, C. E. Thomas, and K.-L. Wong, Nucl. Fusion **26**, 863 (1986).

[17] K. McGuire, J. D. Callen, R. J. Colchin, P. C. Efthimion, E. Fredrickson, K. Hill, V. Paré, W. Park, N. Sauthoff, G. Taylor, R. White, and H. Yamada, in *Proceedings of the 12th European Conference on Controlled Fusion and Plasma Physics* (European Physical Society, Budapest, 1985), Vol. I, p. 134.

[18] K. H. Burrell, S. Ejima, D. P. Schissel, N. H. Brooks, R. W. Callis, T. N. Carlstrom, A. P. Colleraine, J. C. De Boo, H. Fukumoto, R. J. Groebner, D. N. Hill, R.-M. Hong, N. Hosogane, G. L. Jackson, G. L. Jahns, G. Janeschitz, A. G. Kellman, J. Kim, L. L. Lao, P. Lee, J. M. Lohr, J. L. Luxon, M. A. Mahdavi, C. P. Moeller, N. Ohyabu, T. H. Osborne, D.

Overskei, P. I. Petersen, T. W. Petrie, J. C. Phillips, R. Prater, J. T. Scoville, R. P. Seraydarian, M. Shimada, B. W. Sleaford, R. T. Snider, R. D. Stambaugh, R. D. Stav, H. E. St. John, R. Stockdale, E. J. Strait, T. Taylor, J. F. Tooker, and S. Yamaguchi, Phys. Rev. Lett. **59**, 1432 (1987).
[19]J. D. Strachan, in *Proceedings of the Course on Diagnostics for Fusion Reactor Conditions* (Commission of the European Community, Brussels, 1982), Vol. I, p. 383.
[20]W. Stodiek, R. Goldston, N. Sauthoff, V. Arunasalam, C. Barnes, M. Bitter, D. Boyd, N. Bretz, R. Chrien, S. Cohen, P. Colestock, J. Coonrod, S. Davis, D. Dimock, F. Dylla, D. Eames, P. Efthimion, H. Eubank, L. Grisham, R. Hawryluk, E. Hinnov, J. Hosea, H. Hsuan, R. Hulse, D. Hwang, F. Jobes, D. Johnson, R. Kaita, E. Mazzucato, D. McCune, D. McNeill, S. Medley, E. Meservey, D. Mueller, D. Post, W. Roney, G. Schilling, J. Schivell, G. Schmidt, F. Stauffer, L. Stewart, J. Strachan, S. Suckewer, G. Tait, H. Towner, M. Ulrickson, S. von Goeler, D. Voss, and G. Zankl, in *Plasma Physics and Controlled Nuclear Fusion Research, 1980* (IAEA, Vienna, 1981), Vol. I, p. 9.
[21]J. D. Strachan, P. Colestock, H. Eubank. L. Grisham, J. Hovey, G. Schilling, L. Stewart, W. Stodiek, R. Stooksberry, and K. M. Young, Nature **279**, 626 (1979).
[22]J. Hosea, D. Boyd. N. Bretz, R. Chrien, S. Cohen, P. Colestock, S. Davis, D. Dimock, P. Efthimion, H. Eubank, R. Goldston, L. Grisham, E. Hinnov, H. Hsuan, D. Hwang, F. Jobes, D. Johnson, R. Kaita, J. Lawson, E. Mazzucato, D. McNeill, S. Medley, E. Meservey, D. Mueller, G. Schilling, J. Schivell, G. Schmidt, A. Sivo, F. Stauffer, W. Stodiek, J. Strachan, S. Suckewer, G. Tait, H. Thompson, and G. Zankl, in *Plasma Physics and Controlled Nuclear Fusion Research, 1980* (IAEA, Vienna, 1981), Vol. II, p. 95.
[23]J. D. Strachan, T. Nishitani, and Cris W. Barnes, Rev. Sci. Instrum. **59**, 1732 (1988).
[24]S. K. Kim, D. L. Brower, W. A. Peebles, and N. C. Luhmann, Jr., Phys. Rev. Lett. **60**, 577 (1988).
[25]R. E. Chrien and J. D. Strachan, Phys. Fluids **26**, 1953 (1983).
[26]G. Martin, O. N. Jarvis, J. Källne, V. Merlo, G. Sadler, and P. van Belle, Phys. Scr. **T16**, 171 (1987).
[27]R. J. Goldston, R. Kaita, P. Beiersdorfer, G. Gammel, D. L. Herndon, D. C. McCune, and D. D. Meyerhofer, Nucl. Fusion **27**, 921 (1987).
[28]E. L. Bydder, B. S. Liley, and A. H. Morton, Plasma Phys. **21**, 669 (1979).
[29]H. Brysk, Plasma Phys. **15**, 611 (1973).
[30]See National Technical Information Service Document No. ADA 041545 [G. H. Miley, H. H. Towner, and N. Ivich, in NRL Memo Report No. 3332, "NRL Plasma Formulary" edited by D. L. Book (1983)]. Copies may be ordered from the National Technical Information Service, Springfield, VA 22161. The price is $18.95 plus a $3.00 handling fee.
[31]P. L. Colestock, IEEE Trans. Plasma Sci. **PS-12**, 64 (1984).
[32]L. Spitzer, Jr., *Physics of Fully Ionized Gases* (Interscience, New York, 1962), p. 135.
[33]C. S. Chang and F. L. Hinton, Phys. Fluids **29**, 3314 (1986).
[34]H. H. Towner and R. J. Goldston, Bull. Am. Phys. Soc. **29**, 1305 (1984).
[35]R. J. Fonck, R. Howell, K. Jaehnig, L. Roquemore, G. Schilling, S. Scott, M. C. Zarnstorff, M. Bitter, C. Bush, R. Goldston, H. Hsuan, D. Johnson, A. Ramsey, J. Schivell, and H. Towner, submitted to Phys. Rev. Lett. (1989).
[36]T. H. Stix, Nucl. Fusion **15**, 737 (1975).
[37]R. Kaita, R. J. Goldston, P. Beiersdorfer, D. L. Herndon, J. Hosea, D. Q. Hwang, F. Jobes, D. D. Meyerhofer, and J. R. Wilson, Nucl. Fusion **23**, 1089 (1983).
[38]T. J. Murphy and J. D. Strachan, Nucl. Fusion **25**, 383 (1985).
[39]W. W. Heidbrink, Nucl. Fusion **24**, 636 (1984).